



Feasibility study
for neutron inelastic
cross section measurements
at n_TOF/CERN using HPGe detectors

Master Thesis

Maria-Elisso Stamati

Postgraduate Student
Department of Physics, University of Ioannina

May

Contents

<i>Acknowledgements</i>	<i>i</i>
<i>Ευχαριστίες</i>	<i>ii</i>
<i>Abbreviations List</i>	<i>iii</i>
<i>Εκτεταμένη περίληψη</i>	<i>iv</i>
<i>Summary</i>	<i>v</i>
<hr/>	
1	<u>INTRODUCTION</u>
1.1	Motivation 2
1.2	Nuclear Reactions 4
1.3	The first physics case to be studied 8
1.4	Gamma Spectroscopy and HPGe detectors 11
<hr/>	
2	<u>EXPERIMENTAL SET-UP AND TOOLKITS EMPLOYED</u>
2.1	n_TOF facility and experimental set-up 19
2.2	GEANT4 23
2.3	TALYS 26
2.4	ROOT 28
<hr/>	
3	<u>DATA AND ANALYSIS</u>
3.1	HPGe efficiency characterisation 31
3.2	TALYS gamma-production cross section 36
3.3	Yield Calculation Formula 38
3.4	GEANT4 simulation 40
<hr/>	
4	<u>RESULTS</u>
4.1	Results 45
<hr/>	
5	<u>CONCLUSIONS</u>
5.1	Conclusions 51
<hr/>	
6	<u>REFERENCES</u>

6.1	References	53
-----	------------	----

7 APPENDICES

7.1	Appendix A	55
7.2	Appendix B	56
7.3	Appendix C	57
7.4	Appendix D	58
7.5	Appendix E	59

• Acknowledgements

First of all, I would like to express my gratitude to my supervisor Nikolas Patronis for the opportunity he gave me and the trust he showed in me.

Furthermore, I owe a big thank you to my friends and colleagues Zinovia Eleme, Efstathia Georgali and Athanasios Stamatopoulos. They all have been more than willing to help with any practical, computational or even personal problem that I encountered. Another dear friend and colleague I wish to thank is Maria Peoviti, who puts up with me every day in and out of the office.

Lastly, I owe a big wholehearted thank you to my family who have been working tirelessly in the backstage to make this possible for me.

Αρχικά θα ήθελα να ευχαριστήσω τον ακαδημαϊκό μου επιβλέποντα κ. Νικόλαο Πατρώνη για την ευκαιρία που μου έδωσε και την εμπιστοσύνη που μου έδειξε αναθέτοντάς μου αυτή την εργασία.

Θα ήθελα επίσης να ευχαριστήσω τους φίλους και συνεργάτες μου Ζηνοβία Ελεμέ, Ευσταθία Γεωργαλή και Αθανάσιο Σταματόπουλο για την πολύτιμη βοήθειά τους, τόσο σε πρακτικό όσο και σε προσωπικό επίπεδο. Επίσης οφείλω ένα “ευχαριστώ” στη Μαρία Πεοβίτη, φίλη και συνάδελφο, για την υποστήριξή της.

Τέλος, θα ήθελα να ευχαριστήσω από καρδιάς την οικογένειά μου για τη συνεχή και έμπρακτη στήριξή τους από το παρασκήνιο.

• Abbreviations List

α	alpha particle (^4He nucleus)
Al	Aluminium
bpd	bins per decade
CERN	Conseil Européen pour la Recherche Nucléaire
CSG	Constructed Solid Geometry
d	deuterium (^2H)
DWBA	Distorted Wave Born Approximation
EAR1	Experimental Area 1
EAR2	Experimental Area 2
eV	electron Volt
Fe	Iron (Ferrum)
FWHM	Full Width at Half Maximum
Ge	Germanium
GEANT	Geometry And Tracking
H	Hydrogen
He	Helium
HPGe	High Purity Germanium
n	neutron
n_TOF	neutron Time Of Flight
p	proton
PS	Proton Synchrotron
t	tritium (^3H)

Σκοπός αυτής της εργασίας είναι να διερευνήσει κατά πόσον η εγκατάσταση ενός σταθμού φασματοσκοπίας γ στο πείραμα n_TOF του CERN είναι ικανή να παράξει αποτελέσματα ενεργού διατομής ανελαστικής σκέδασης νετρονίων, καθώς και η διερεύνηση της γεωμετρίας του σταθμού. Ως μία ενδεικτική πρώτη αντίδραση χρησιμοποιήθηκε η ανελαστική σκέδαση νετρονίων στο σίδηρο-56, καθώς υπάρχουν πειραματικά δεδομένα για τον έλεγχο της πορείας της μελέτης, όμως είναι χρήσιμο να ελεγχθούν και να εμπλουτιστούν, δεδομένου ότι ο σίδηρος είναι ένα ευρέως χρησιμοποιούμενο υλικό σε μηχανικά εξαρτήματα.

Η μελέτη σκοπιμότητας πραγματοποιήθηκε κυρίως μέσω του GEANT4, ενός πακέτου προσομοίωσης της πορείας της ακτινοβολίας μέσα στην ύλη. Το GEANT4 δίνει τη δυνατότητα στον προγραμματιστή να αναπαράξει τη γεωμετρία του προβλήματός του αλλά και τις φυσικές διεργασίες που λαμβάνουν χώρα. Στην παρούσα εργασία, το υπολογιστικό πακέτο χρησιμοποιήθηκε αφ'ενός για το χαρακτηρισμό του ανιχνευτή υπερ-υψηλής καθαρότητας γερμανίου EGPC 25S/N 54035 της εταιρίας CANBERRA ως προς την απόδοσή του και αφ'ετέρου για την προσομοίωση της ανελαστικής σκέδασης των νετρονίων της δέσμης του n_TOF από στόχο σιδήρου. Πρόκειται για έναν πρωτότυπο ανιχνευτή με το κύκλωμα του προ-ενισχυτή του να είναι ειδικά σχεδιασμένο ώστε να επιτρέπει τη βέλτιστη λειτουργία του ανιχνευτή στις ειδικές συνθήκες των πειραματικών αιθουσών της εγκατάστασης n_TOF .

Αρχικά πραγματοποιήθηκε ο χαρακτηρισμός του ανιχνευτή, διαδικασία που αποτελείται από δύο στάδια. Το πρώτο είναι η λήψη πειραματικών δεδομένων απόδοσης με πηγή βαθμονόμησης ενώ το δεύτερο είναι η αναπαραγωγή αυτών των δεδομένων μέσω του GEANT4, μεταβάλλοντας τις χαρακτηριστικές παραμέτρους της προσομοίωσης μέχρι να επιτευχθεί η καλύτερη δυνατή συμφωνία.

Στη συνέχεια υπολογίστηκε ο αναμενόμενος αριθμός καταγεγραμμένων γεγονότων στον ανιχνευτή. Για τον υπολογισμό αυτόν αξιοποιήθηκε ο κώδικας TALYS, ένας κώδικας για θεωρητικούς υπολογισμούς πάνω σε πυρηνικές αντιδράσεις. Συγκεκριμένα, ο κώδικας TALYS χρησιμοποιήθηκε για την εξαγωγή των θεωρητικών τιμών της ενεργού διατομής για την παραγωγή των ακτίνων γ που έπονται της ανελαστικής σκέδασης. Τα αποτελέσματα αυτά, σε συνδυασμό με την τιμή της απόδοσης του ανιχνευτή στις συγκεκριμένες ενέργειες, όπως υπολογίστηκε μετά το χαρακτηρισμό αυτού, οδηγούν στον υπολογισμό των γεγονότων που αναμένεται να καταγραφούν.

Επιπλέον του υπολογισμού των γεγονότων, πραγματοποιήθηκε η ολική προσομοίωση της ανελαστικής σκέδασης, λαμβάνοντας υπόψιν τις διαφορετικές ενέργειες των νετρονίων της δραστηριότητας n_TOF , όπως δίνονται από τις μετρήσεις της ροής της δέσμης, αλλά και περιορισμών της γεωμετρίας λόγω της ανάγκης ολοκλήρωσης της διαφορικής ενεργού διατομής που μετράται. Το τελικό φάσμα της προσομοίωσης δίνει πληροφορίες για το μέγεθος και το είδος του υποβάθρου, πέραν των γεγονότων στις αναμενόμενες φωτοκορυφές.

In this work, it is investigated whether a γ spectrometry set-up installed in n_TOF can aid to the acquisition of neutron inelastic cross section data and its geometrical configuration is examined. To achieve this, the p-type coaxial HPGe detector EGPC 25S/N 54035 by CANBERRA was characterised in terms of its efficiency by a series of efficiency measurements that took place in the n_TOF old control room at CERN. The characterised GEANT4 model of the detector was then used in simulation to inspect the spectrum expected after a real-life experiment of neutron inelastic scattering. Furthermore, the counts expected to be recorded were estimated using the TALYS code for the cross section calculation.

- INTRODUCTION -

- ☒ *Motivation*
- ☒ *Nuclear Reactions*
- ☒ *The first physics case to be studied*
- ☒ *Gamma Spectroscopy and HPGe detectors*

1.1 - Motivation

Neutron inelastic scattering cross section data play a significant role in the fields of nuclear research as well as nuclear technology. Some prominent examples concerning the latter are new generation nuclear power reactors, transmutation of nuclear waste and shielding applications. Inelastic scattering is followed by the emission of γ -rays, when the residual nucleus decays to its ground state. The production cross section of these γ -rays plays an important role on dosimetry and radioprotection. It can also lead to the total inelastic cross section or some lower and upper bounds.

It is thus important to have many and well evaluated data sets, covering as wide an energy range as possible. The n_TOF facility at CERN provides a neutron beam stretching from the meV to the GeV region, making it a viable candidate for the development of a powerful γ spectrometry set-up. Before such a set-up can be assembled, several tests and simulations must be performed in order to determine the optimal configuration in both geometry and instrumentation.

The aim of this work is to characterise n_TOF's prototype HPGe detector, estimate the counting rate expected from a typical experiment and create a GEANT4 simulation to inspect the role of the geometry on the final spectrum.

1.2 - Nuclear Reactions

Nuclear Reaction Categories:

All types of nuclear reactions can be divided into two major categories: direct reactions and compound nucleus reactions. This division holds when either the reaction time or the number of intra-nuclear collisions is considered. Direct reactions take place over a much shorter amount of time and consist of as few as one or two intra-nuclear collisions. In this case, the projectile only interacts with the outermost nucleons of the target nucleus. On the other hand, the compound nucleus reactions require more time, as the statistical nature of the reaction has increased and the projectile interacts with the target nucleus with many intra-nuclear collisions. This increase in the statistical nature of the reaction causes the decrease in the coupling between the incident and outgoing channels, leading to the Bohr Independence Hypothesis, which states that the “memory” of the incident channel is lost in the case of compound nucleus reactions.

A particle can also be emitted in intermediate time scales that do not fit in either of the two aforementioned categories, thus hinting the existence of a mechanism that embodies both direct- and compound- like features. This is the case of pre-equilibrium emission, which takes place after the projectile has interacted with a few of the target nucleus’ nucleons but before statistical equilibrium is reached, with statistical equilibrium meaning that the projectile’s energy has been equally distributed among all of the target nucleons.

In terms of the projectile’s energy, the compound nucleus mechanism is predominant in the lower energy range, while direct reactions prevail for higher projectile energies. Pre-equilibrium emission takes place in an intermediate range, typically above 10MeV and up to a few hundred MeV. This is summarised in Figure 1.1.

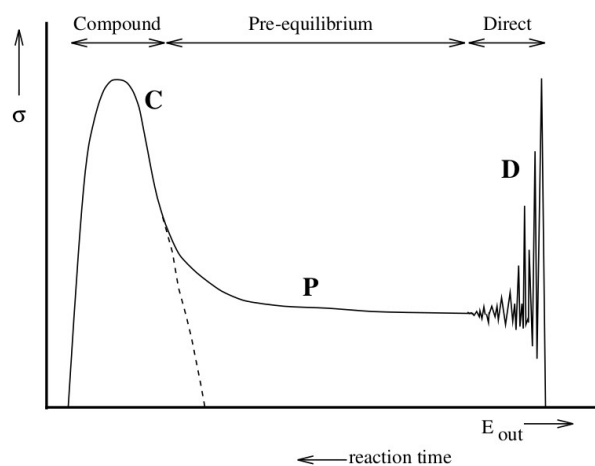
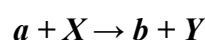


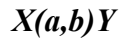
Figure 1.1: Schematic representation of a reaction cross section curve shape and predominant mechanisms according to the reaction time and energy.

Formalism:

In terms of formalism, a nuclear reaction is written as



or, in a more compact form, as



where a represents the projectile, X the target nucleus, b the ejectile and Y the residual nucleus.

Scattering:

A major type of nuclear reaction is scattering. Scattering occurs when the projectile and ejectile (a and b when following the above formalism) are the same particles and, correspondingly, the target and residual nuclei (X and Y) are the same, although not necessarily in the same state as before the reaction.

When both the ejectile (b) and the residual nucleus (Y) remain in their ground state after the reaction, the scattering is called “elastic”, whereas if one or both of them are in an excited state, the scattering is characterised as “inelastic”.

Other types of reactions are capture -where the projectile is being “absorbed” by the target nucleus forming a different nucleus in an excited state, that later decays to its ground state-, pick-up and stripping reactions, fission, (n,xn), etc.

Models:

In nuclear physics, there is not one fundamental theory used to interpret all the possible phenomena occurring. It is discussed in a phenomenological approach with a different formulation applying to each type of phenomenon. There are models that describe direct reactions, such as the optical model and the Distorted Wave Born Approximation (DWBA), while different models describe compound nucleus reactions, such as the Hauser-Feshbach theory, etc. One of the most commonly used models and approximations, and one that has been used in this study, is the optical model that will be discussed below.

The optical model:

The optical model is an approximation mostly useful for studying an average behaviour in reactions such as scattering. It is represented by a complex potential, with its real part being responsible for elastic scattering and its imaginary part being responsible for the absorption.

$$U(r) = V(r) + iW(r), \text{ with } W < 0$$

The real part, $V(r)$, may be very similar to a shell-model potential, since it describes the interaction between a projectile and a target nucleus. The imaginary part, $W(r)$, can have different forms, depending on the incident particle’s energy. If low, the projectile’s energy is absorbed by the “valence” nucleons, so $W(r)$ must be large only near the surface of the nucleus. In this case, it is usually chosen to be proportional to dV/dr . An example of such a potential is given in Figure 2.1. At higher energies, $W(r)$ changes form, as the inner nucleons participate in the absorption as well. Optical potentials also include spin-orbit terms and a Coulomb term, if the projectile is a charged particle.

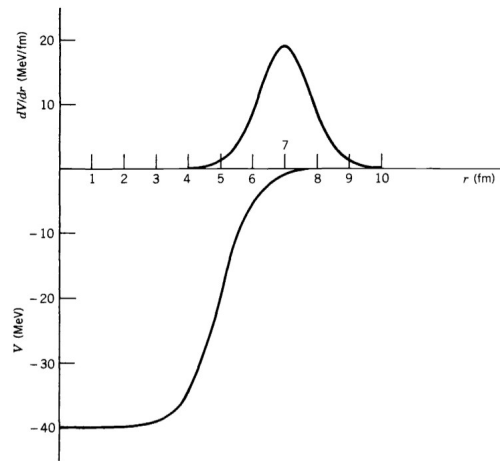


Figure 1.2: Example of optical potential: Shell model-like $V(r)$ (below) and $W(r) \sim dV/dr$ (above).

The implementation of the optical model thus consists of the choice of potential and the numerical solving of the Schrödinger equation for this potential.

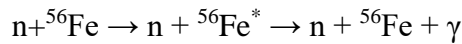
If we take the optical model calculations and account for the fact that the incident and outgoing waves are distorted by the nucleus, we arrive at another model, the *Distorted Wave Born Approximation* [1 - 3].

1.3 - The first physics case to be studied

In order to establish the final configuration of the γ spectrometry set-up, a sample case has to be chosen for simulation and then for future experimental measurement. For this work, the physics case chosen to be studied is the inelastic scattering of neutrons on ^{56}Fe from a natural iron target. This choice was made upon certain criteria: Iron is a material commonly used in apparatus, thus its cross section for neutron induced reactions is an important quantity to be extensively studied. There are experimental data available so that the simulations can be cross-checked and an iron target is not too hard to manufacture.

The $n+^{56}\text{Fe}$ reaction channels:

When bombarding ^{56}Fe with neutrons, several reactions can take place. The one of interest to this study is the inelastic channel, which could be written down as



with ^{56}Fe ending up in an excited state by definition of the inelastic scattering.

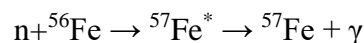
A relatively easily measurable quantity of the above reaction is the γ -rays resulting from the de-excitation of $^{56}\text{Fe}^*$. Analysing the γ spectrum, we can extract the probability of each γ -ray being produced, called the γ production cross section, and, seeing how the γ production cross section is a measure of the total cross section leading to a particular state, by combining this information with the isotope's decay scheme, we can draw conclusions about the total inelastic scattering cross section. If one was able to measure all γ -rays from the de-excitation of every one of ^{56}Fe excited states, one could calculate exactly the inelastic cross section. This being extremely complicated in terms of exact knowledge of the decay scheme as well as being very difficult by means of experimental equipment, one can only measure some of the γ -rays and extract bounds for the total cross section [4 - 6].

The energy of the strongest γ -rays coming from the de-excitation of the first excited states of ^{56}Fe as well as the states connected by these transitions are given in Table 1.1.

γ -ray Energy (keV)	Initial Level Energy (keV)	Initial Level J^π	Final Level Energy (keV)	Final Level J^π
846.8	846.7	2^+	0.0	0^+
1238.3	2085.1	4^+	846.7	2^+
1810.8	2657.6	2^+	846.7	2^+
2094.9	2941.5	0^+	846.7	2^+

Table 1.1: Energies of the γ -rays resulting from the decay of the first excited states of ^{56}Fe [7]

Other channels for the $n+^{56}\text{Fe}$ reaction are elastic scattering and neutron capture. In the first case, ^{56}Fe remains in its ground state and the only particle that can be detected is the neutron. In the case of neutron capture, $^{57}\text{Fe}^*$ is produced and later on de-excites emitting a γ -ray, as denoted below:



The resulting γ -rays correspond to the energy difference of the ^{57}Fe excited states and are recorded as well. The first few excited states of ^{57}Fe and the strongest γ -rays from their decay are presented in Table 1.2.

γ -ray Energy (keV)	Initial Level Energy (keV)	Initial Level J^π	Final Level Energy (keV)	Final Level J^π
14.4	14.4	$3/2^-$	0.0	0^+
122.1	136.5	$5/2^-$	14.4	$3/2^-$
352.4	366.8	$3/2^-$	14.4	$3/2^-$

Table 1.2: Energies of the γ -rays resulting from the decay of the first excited states of ^{57}Fe [7]

Irradiating a natural iron target:

For an actual experiment, it is less costly and less complicated to use an iron target of natural composition. The isotope of interest, ^{56}Fe , has an abundance of 91.7%, so the target is mostly composed of it. However, there are still some small amounts of other iron isotopes, so more reactions will take place and the resulting spectrum will show more photopeaks as well as more background energy deposition coming from scattered neutrons.

The isotopic composition of natural iron is summarised in Table 1.3.

Isotope	Abundance (%)
^{54}Fe	5.845
^{56}Fe	91.754
^{57}Fe	2.119
^{58}Fe	0.282

Table 1.3: The isotopic composition of natural iron [7].

We can expect that the most prominent photopeaks will result from the (n, γ) and $(n, n'\gamma)$ reactions on ^{54}Fe and ^{57}Fe isotopes, thus their energies will correspond to the decay of the ^{54}Fe , ^{55}Fe , ^{57}Fe and ^{58}Fe excited states.

1.4 - Gamma Spectroscopy and HPGe detectors

Interaction of photons with matter:

The mechanisms of photon interaction with matter that play a role in radiation measurements are three: photoelectric absorption, Compton scattering and pair production. These lead to the transfer of all or part of the photon energy to electron energy.

In the photoelectric process, a photon is captured by an atom, which, in return, emits an energetic photoelectron, originating from the atom's tightly bound shells, mostly its K-shell. In addition to this photoelectron, the interaction leaves behind an ionised atom with a vacancy in one of its bound shells. This vacancy is filled up through the capture of a free electron or by the rearrangement of the atom's electrons, leading to the emission of one or more characteristic X-rays.

Compton scattering takes place between the incident photon and an electron in the absorbing material. The photon is scattered on the electron and its direction changes while a portion of its energy is transferred to the electron. This portion depends on the angle and it can vary from zero to almost all of the photon energy. A schematic representation of the Compton scattering process, along with the formula used to calculate the scattered photon's energy, is given in Figure 1.3.

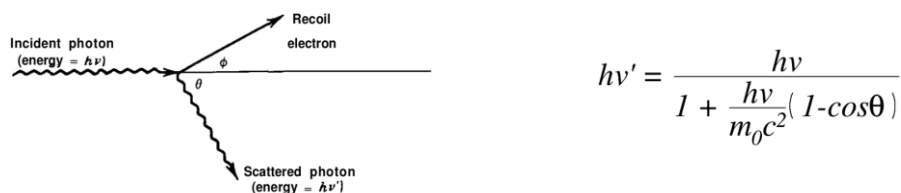


Figure 1.3: A schematic representation of the Compton scattering process (left) along with the formula giving the energy of the scattered photon (right).

Pair production is possible if the photon energy exceeds 1.02MeV, namely twice the rest-mass energy of an electron, but is a predominant mechanism only for high-energy photons, with energy above several MeV. It is a reaction that can only take place in the Coulomb field of a nucleus and it leads to the creation of an electron-positron pair in place of the original photon. All the photon energy above the 1.02MeV needed for the creation of the pair is shared by the electron and the positron as kinetic energy. Very soon, the positron will interact with an electron in the absorbing material and will annihilate, producing two photons [8 - 10].

The energy range at which each mechanism is predominant is given in Figure 1.4.

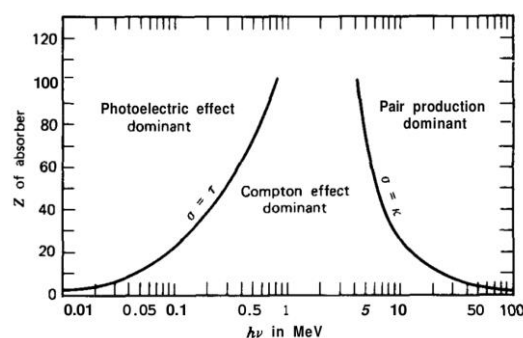


Figure 1.4: The predominant photon interaction mechanisms with regards to their energy.

Interactions of neutrons with matter:

Neutrons carry no electric charge and are capable of travelling many centimetres of matter without any type of interaction. As a result, they can be completely invisible to a detector of typical size. When they do participate in interactions, it is with a nucleus of the absorbing material. The neutron can be fully absorbed by that nucleus and replaced by other types of radiation or it can be scattered, changing its direction and transferring part of its energy to the material.

For low energy neutrons, referred to as thermal neutrons, the most probable reaction is neutron capture, while the probability for scattering as well as neutron induced reactions such as (n, a), (n, xn), etc, increases with the energy of the incident neutron [8].

Semi-Conducting materials:

Electrons within a solid exist only in allowed energy bands, regions of many discrete levels so closely spaced that they can be considered a continuum, separated by forbidden energy regions or gaps. The lower energy band is called the “valence band” and corresponds to the outermost shell electrons. The next band, lying above the valence band, is the “conduction band” and it represents the electrons that are free to move around in the crystal lattice, as they are fully detached from their atoms. It owes its name to the fact that these electrons are the ones that contribute to the material’s conductivity.

These two bands are separated by the “bandgap”, the size of which is used to classify the material in one of the three material categories: insulator, semi-conductor and conductor. For the case of a conductor, the band gap is non-existent, thus it’s always characterised by high electrical conductivity. Insulators and semi-conductors on the other hand, have a finite value of a bandgap and their electrons must have sufficient energy so to cross it and reach the conduction band in order for the material to exhibit conductivity. For insulators, the bandgap is usually higher than 5eV while for semi-conductors it is much lower. The classification of solids according to their bandgaps is summarised in Figure 1.5.

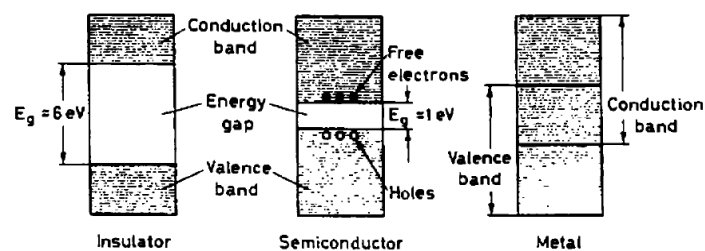


Figure 1.5: Conduction, valence bands and bandgaps for the three categories of solids: Insulators (left), Semi-Conductors (middle) and Metals (right).

If a valence electron gains sufficient energy, it can cross the bandgap and reach the conduction zone. This excitation creates an electron in the conduction band and leaves a vacancy, called hole, back to the valence band. This hole represents a net positive charge. Both the hole and the electron can move if an external electrical field is applied.

An electron-hole pair can be created even by thermal energy, depending on the material’s bandgap. The probability of it happening is given by

$$p(T) = CT^{3/2} \exp\left[-\frac{E_g}{2kT}\right]$$

with the absolute temperature denoted as T, k being the Boltzmann constant, E_g the material's bandgap and C a proportionality constant depending on the material. We can see that the probability largely depends on the ratio of the bandgap to the temperature.

The most commonly used semi-conducting materials are Si and Ge, with a bandgap of $\sim 1\text{eV}$.

Basics of semi-conductor detectors:

The basis of semi-conductor detectors lies with the formation of a “junction” or, as they are also known in electronics, a “diode”. A simple such configuration is the pn junction, formed by bringing a p-type material in contact with an n-type material, as shown in Figure 1.6. This classification of the material has to do with the type of impurities it contains. An impurity is an atom of different valency that can replace an atom of the lattice and disturb the electronic balance. The net character of the material depends on the type of impurity that is in excess. If the impurity is an atom of higher valency than the lattice, providing an extra electron to the whole electronic configuration, the material is characterised as n-type. On the other hand, if the impurity is a lower valent atom resulting in a “hole”, one electron too few to maintain the electronic configuration, the material is referred to as p-type. When bringing these two different materials in contact, a diffusion starts to take place at the intersurface because of the difference in the concentration of electrons and holes. Electrons drift towards the p region filling up holes, while holes diffuse to the n side capturing electrons. This recombination causes a charge build-up on each side and an electric field is created halting further diffusion. This field also causes a potential difference, known as “contact potential”.

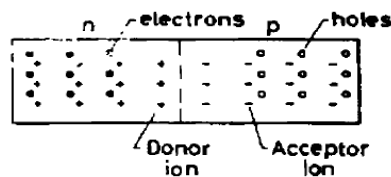


Figure 1.6: A pn junction, simplified.

The intermediate region where the diffusion first started is the region where the change in the potential occurs and it's called the “depletion region”. It has the property of being devoid of all charge carriers. Any electron or hole created in the depletion region is swept out of it by the electric field, and this is exactly the characteristic that leads to the junction's use as a detector: Ionising radiation entering the depletion region creates electron-hole pairs (a process called ionisation) that are then swept out. If we add electrical contacts on the ends of the junction we can collect these charge carriers and detect a current signal. The depletion region is called the “active volume” of the detector, as it is the region of the junction from where carriers corresponding to interactions can be collected and studied.

The current we detect is proportional to the ionisation and we can connect it to the energy of the incident particle, because the energy required to create one electron-hole pair is independent of both the energy and the type of the incident particle.

HPGe detectors:

In order to extract all possible information about the incident photons, detectors rely on a series of basic steps of operation: The conversion of the energy of the photons into kinetic energy of electrons through one of the main processes of photon interaction with matter, the production of electron-ion pairs, and finally, their collection and measurement. Seeing how gamma rays are highly penetrating radiation, the active volume of the detector has to be large enough for their whole energy to be converted into electron kinetic energy. The thickness of the depletion region of a simple junction is given by:

$$d = \left(\frac{2\epsilon V}{eN} \right)^{1/2}$$

where ϵ is the dielectric constant, V the reverse bias voltage, e the electron charge and N the net impurity concentration of the material.

In order to increase the junction depletion depth for a given bias voltage, the net impurity concentration must be further reduced. This can be achieved in two ways: Either with new refining techniques that reduce it to 10^{10} atoms/cm³ or by balancing the residual impurities by an equal concentration of dopant atoms of the opposite type. In this event of exact cancellation of impurity types, the material is called compensated. Detectors manufactured in the first way are referred to as High Purity Germanium detectors, or HPGe detectors, while detectors manufactured by the second method are mostly Ge(Li) detectors, because the most common manufacturing process is lithium ion drifting. In a Ge(Li) detector, the temperature of the crystal must in all times be kept very low (liquid nitrogen temperature, i.e. 77K), a fact that imposes many practical difficulties and gradually leads to the extinction of the Ge(Li) detector.

To minimise the number of impurities and to create high purity germanium crystals, the initial material is locally heated and a molten zone is created and passed from one end to the other. Impurities are more soluble in molten germanium, so they are transferred to the molten zone and subsequently removed from the material. The resulting crystal is of ultrahigh purity, with minimal impurities remaining. If these impurities are donor atoms, meaning that the impurity is a five valent atom, such as phosphorus or arsenic, the material is referred to as high purity n-type germanium, whereas if acceptor impurities remain, such as three valent gallium or boron, the material is referred to as high purity p-type germanium.

The core of an HPGe detector is the crystal. The active volume of the detector is the high purity crystal, fabricated as described above. On top of the crystal, donor or acceptor atoms are implanted or diffused, forming the n⁺ and p⁺ contact respectively. The most common materials used are boron, for the production of the p contact, and lithium, for the production of the n contact. To operate the detector, reverse bias voltage is applied to these contacts.

Depending on their geometry, HPGe come in different configurations: The planar, the true coaxial, the closed-end coaxial and the well, as shown in Figure 1.7 below:

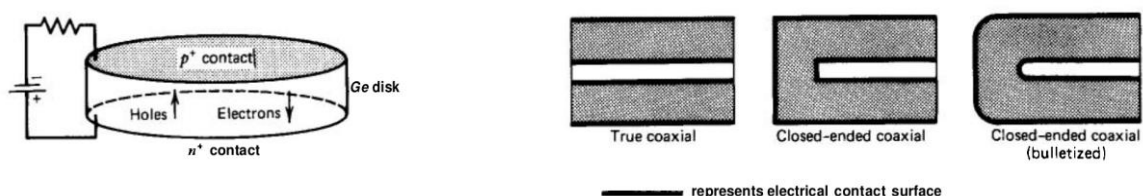


Figure 1.7: Schematic representation of the most commonly used HPGe configurations, planar (left) and coaxial (right)

Planar detectors were the first to be produced, as they are the simplest type to manufacture. However, they are bound to have a small active volume, so a new geometry had to be developed in order to increase it. True coaxial detectors are cylindrically symmetric and have much larger active volumes. One electrode is fabricated on top of the crystal surface, while the second is fabricated along its inner surface after the core has been removed. True coaxial detectors, though, lack in efficiency and closed-end coaxial detectors were developed in order to increase the sensitive volume near the radioactive source being measured. This is achieved by only removing part of the core to fabricate the inner contact and extending the outer contact on the front flat surface of the crystal. To further optimise the detector, its front edge is rounded to improve charge collection. This procedure is referred to as “bulletisation”.

The thickness of the contacts produces an insensitive layer from which charge carriers are not collected, thus called the “dead layer” of the detector. A typical lithium n+ contact causes a dead layer of about 700 μm , while the dead layer caused by an ion-implanted p+ contact is only about 0.3 μm thick.

Energy resolution and Detection efficiency:

There are two very important factors in spectroscopy: The energy resolution of a detector and its detection efficiency. The resolution is usually given in terms of full width at half maximum (FWHM) and it determines the extent to which the detector can distinguish two energy peaks lying close to each other. Peaks lying closer than their FWHM, denoted sometimes as ΔE , are considered unresolvable. The relative resolution at an energy E is given by

$$R = \frac{\Delta E}{E}$$

HPGe detectors have a very good energy resolution, meaning that, if we send a monoenergetic beam of radiation into the detector, the resulting spectrum will have a peak of small width, resembling the sharp delta-function peak we would ideally expect. Other detectors, such as NaI scintillators, have much worse energy resolution and their resulting spectrum would exhibit a very wide peak instead, as shown in Figure 1.8.

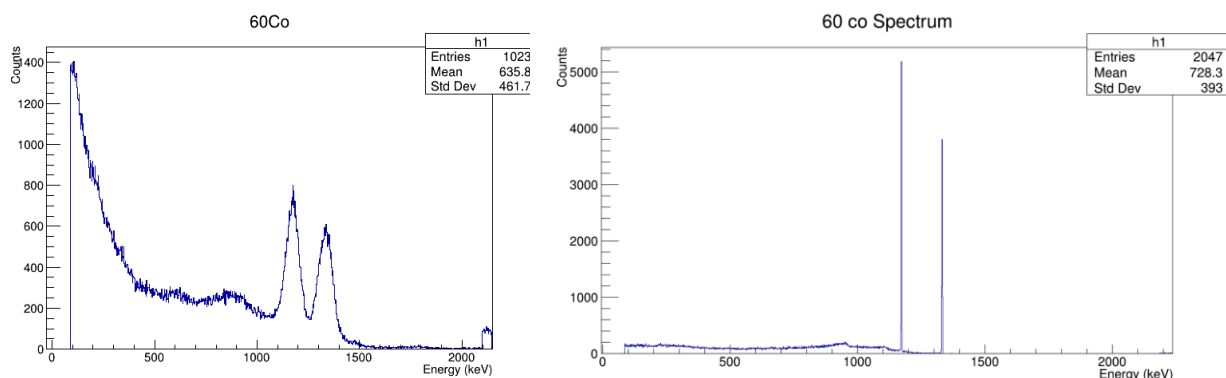


Figure 1.8: A γ -spectrum with a ^{60}Co radioactive source acquired with a NaI (left) and a HPGe (right). The NaI has a much worse energy resolution with much wider peaks.

When it comes to the detection efficiency, we have to differentiate the total efficiency from the photopeak efficiency. The total efficiency is connected to the number of photons that deposited

any amount of energy in the crystal, while the photopeak efficiency is connected to the number of photons whose energy was recorded in the photopeak. The latter is the most commonly used type of efficiency in γ -spectrometry and is usually referred to simply as “efficiency”. It can be divided into two categories: the intrinsic efficiency and the absolute efficiency. The absolute efficiency is defined as the fraction of the events emitted by the source that are actually recorded in the detector:

$$\epsilon_{abs} = \frac{\textit{events recorded}}{\textit{emissions}}$$

This heavily depends on the geometrical configuration of the set-up and the dimensions of the detector, but also on the detector itself and the interaction of the incident radiation with its material. We can gather all the geometrical parameters in a separate factor, usually referred to as G , and then all that remains is the intrinsic efficiency of the detector [8 - 11].

$$\epsilon_{abs} = \epsilon_{intr} * G$$

with $G = \Delta\Omega/4\pi$ ($\Delta\Omega$ used to denote the solid angle the detector covers) and

$$\epsilon_{intr} = \frac{\textit{events recorded}}{\textit{events incident on the detector}}$$

- EXPERIMENTAL SET- UP AND TOOLKITS EMPLOYED -

-
- ✕ *n_TOF facility and experimental set-up*
 - ✕ *GEANT4*
 - ✕ *TALYS*
 - ✕ *ROOT*

2.1 - n_TOF facility and experimental set-up

The n_TOF facility at CERN is designed to study neutron induced reactions, bearing importance for research fields ranging from stellar nucleosynthesis to applications of nuclear technology. Its neutron beam is generated by spallation, when a pulsed proton beam from CERN's PS accelerator hits a lead target. For every proton, about 300 neutrons are produced. The beam is slowed down by the lead target itself, as well as by a water slab in front of it. The resulting neutron spectrum is very wide, stretching from the meV to the GeV region. The kinetic energy of the neutrons is precisely determined via time-of-flight technique, to which n_TOF owes its name. n_TOF consists of 2 evacuated flight paths and consequently 2 experimental areas, EAR1 and EAR2. The first flight path is almost horizontal with a length of 185m and leads to EAR1, while the second flight path, leading to EAR2, is vertical and has a length of 20m. The flight paths are presented in graphical form in Figure 2.1, along with a graphical representation of CERN's accelerator complex. Before it reaches the EAR, the beam is collimated. n_TOF uses two different types of collimators, the capture collimator, with a diameter of ~ 2 cm, and the ~ 8 cm in diameter fission collimator, depending on each experiment's needs in flux.

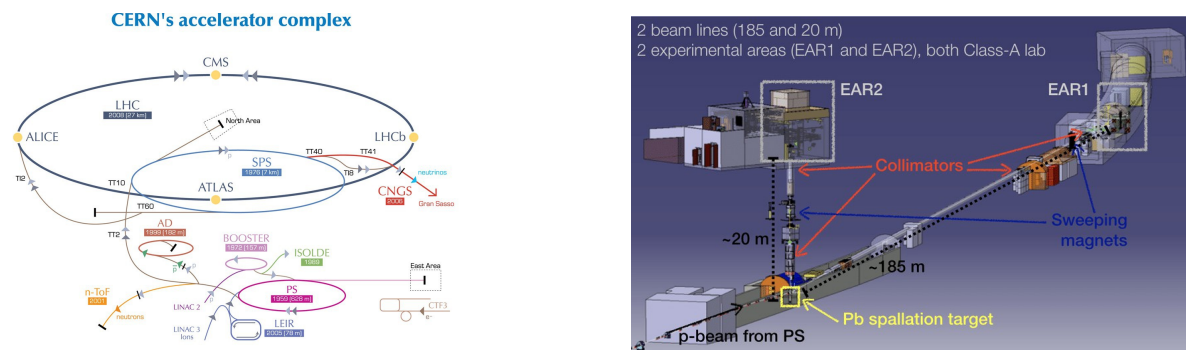


Figure 2.1: CERN's accelerator complex (left) with n_TOF represented by the colour yellow (lower left corner) and a schematic diagram of n_TOF's flight paths and EARs.

A typical experiment is performed by placing a sample in the neutron beam, with one or more detectors around it to measure the products of the reaction. The ultimate goal is to extract the reaction cross section as a function of the incident neutron energy, which is why the wide energy range of neutrons is extremely useful [12].

This feasibility study aims at the development of a γ -ray spectroscopy set-up, with the use of HPGe detectors, the number of which needs to be determined. Their number greatly affects the geometry of the set-up. When measuring the photons resulting from the reaction of interest, one can only record the portion of the photons that reach the detector and thus can deduce only a "portion" of the total γ -ray production cross section. This portion is the differential cross section and it can be used as an intermediate step to calculating the total cross section via the Gaussian Quadrature method.

The Gaussian Quadrature, as its name suggests, is a method of numerical integration. Numerical integration is used to evaluate a definite integral to a desired level of precision, and is mostly used in cases where either there is no closed-form expression for the integral, or when the function to be integrated is not explicitly known. For example, the simplest such approximation is the trapezoidal rule, which states that the area below the unknown function $f(x)$ from a point $x=a$ to a point $x=b$ is approximately equal to the area of the trapezoid formed by connecting the points a , b , $f(a)$ and $f(b)$, as shown in Figure 2.2. To make the approximation even more accurate, we can increase the number of trapezoids we draw.

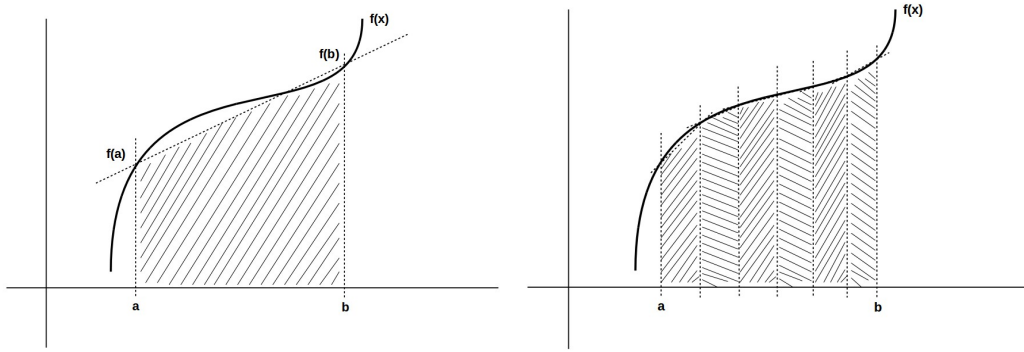


Figure 2.2: The trapezoidal rule for a function $f(x)$ with one trapezoid (left) and with many trapezoids with a smaller step (right).

The Gaussian Quadrature method allows us to find another function, different but known, and a set of weighing factors that, combined with the new function's value at some particular abscissas, can give us the value of the original integral.

Written in mathematical form,

$$\int_{-1}^{+1} f(x)dx = \sum_{j=1}^n w_j f(x_j)$$

where the left hand side consists of the integral we want to know and the right hand side contains the function (f), the abscissas (x_j) and weighing factors (w_j). The method can work for any interval and with another weighing factor (w) in the unknown function as well, but we limit our study to the case of $[-1, +1]$ and $w=1$ since this is the case that corresponds to our cross section deduction problem.

The abscissas and the weighing factors are the free parameters of the problem and are calculated based on the fact that we want the error of the above approximation to be zero. This error is simply

$$E_n(f) = \int_{-1}^{+1} f(x)dx - \sum_{j=1}^n w_j f(x_j)$$

and the set of equations of it being equal to zero can be solved by employing a base of orthogonal polynomials in the interval of integration. For the $[-1, +1]$ interval, these polynomials are the Legendre polynomials [13].

In our specific case, the unknown function f is the differential cross section $d\sigma/d\Omega$, of which we only know a few values, with their number depending on the number of detectors used in an experiment. If we only use one detector, then we only know one value of the differential cross section, but if we have two detectors at our disposal we can measure its value for two different angles, etc.

When applying this mathematical method to our cross section problem, we can get the exact angle (it corresponds to the abscissa) in which the detectors need to be placed according to their number as well as the weighing factors. This is given in Table 2.1 below [4].

Number of Detectors	One detector	Two detectors		Three detectors		
Detector #	1	1	2	1	2	3
Angle (deg)	54.75 or 125.26	30.56 or 149.44	70.12 or 109.88	76.19 or 103.81	48.61 or 131.39	21.18 or 158.82
Weight	2	0.69571	1.30429	0.93583	0.72152	0.34265

Table 2.1: The possible angles the detectors need to be placed in order to apply the Gaussian Quadrature method to obtain the angle integrated cross section, according to their number. Also, the weighing factors needed to implement the method.

To choose one of the two possible angles for the installation of the detector, the physicist must also take into account other aspects of their experiment, set-up and facility. For a TOF facility, it is most common to place the detectors at backward angles so as to minimise their exposure to γ -flash. γ -flash is a term used to describe relativistic particles and photons that are being produced along with the neutron beam. This causes a big amount of energy to be deposited in the detector, even before the neutron beam reaches the target and the reactions of interest begin to take place. It has been proved by experimental tests and simulations alike that the effect of the γ -flash on the detector is less if the detector is placed at a backward angle.

In the case of CERN's n_TOF, such a comparison has been simulated and presented in a meeting [14], as shown in Figure 2.3.

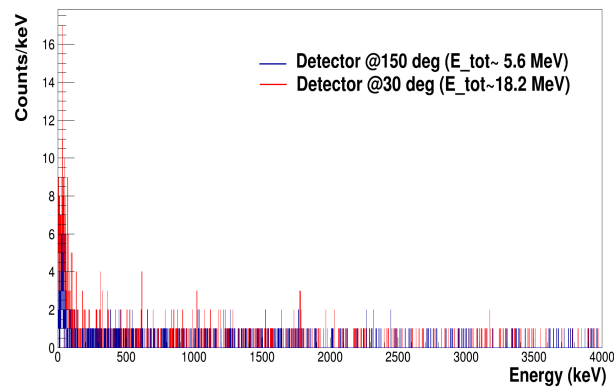


Figure 2.3: Comparison of the total energy deposition in the HPGe detector when placed in a forward (red) and backward (blue) angle with regards to the n_TOF neutron beam in EAR1.

2.2 - GEANT4

GEANT4 [5] is a widely used simulation toolkit for the passage of particles through matter. It utilises a plethora of physical models as well as experimental data in order to handle all physical processes -electromagnetic, hadronic, optical, etc.- that arise from the tracking of particles and their interaction with matter. It covers a wide energy range and is employed in many different fields, from nuclear and high energy physics to astrophysics to biology. GEANT4 is engineered using object-oriented technology and is implemented in the C++ programming language. It also provides visualisation options [16].

In order to run a simulation, the user has to define the geometry of their physical problem and the primary particles that will be passed. Considering the geometry, GEANT4 functions using different volumes to “build” the simulation. Each volume used is created by describing its shape and its physical characteristics and then placing it inside a containing volume. This is achieved through the concepts of “logical volume”, “physical volume” and “solid”. A solid in GEANT4 is an object of specific shape and dimensions. The logical volume includes all the geometrical properties of the solid and adds to it the physical characteristics, such as its material. Finally, the physical volume is the placed instance of the logical volume, meaning that it places it inside a containing volume, referred to as “mother volume”, and includes its coordinates, rotation details etc. The largest volume that contains all other volumes is named “World”. If a mother volume is rotated, all its “daughter volumes”, i.e. the volumes it contains, will be rotated in the same way, since all the details of a daughter volume’s placement are relative to the mother volume and not the World volume.

GEANT4 uses the Constructed Solid Geometry (CSG) technique to model its primitive solids. Being described by the minimal possible number of parameters, the CSG primitives GEANT4 offers are Boxes, Tubes and their sections, Cones and their sections, Spheres, Wedges, and Toruses. Some of these primitives are depicted in Figure 2.4. To construct more complex solids, the user can apply boolean operations (union, intersection, subtraction) on these primitives.

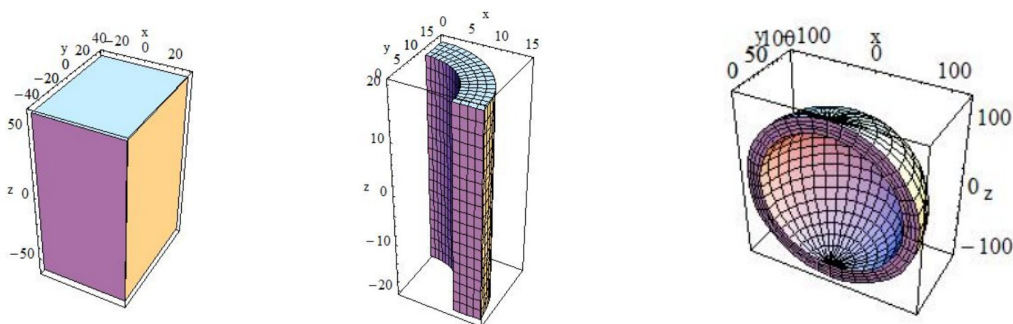


Figure 2.4: Some of the primitives offered by GEANT4: A box (left), a section of a tube (middle) and a spherical section (shell) (right).

Next, the user has to attribute all the desired properties to the primary particles. Being object oriented, GEANT4 contains classes that control all its basic functions. This goes to the generation of primaries as well, with the responsible class being `G4PrimaryGenerationAction`. Using this class, the user can randomise and provide the initial values of a particle (type, position, energy, momentum, etc.) and assign them via the primary generator, as the primary generator “shoots” one particle of assigned energy from an assigned initial point to an assigned direction. The most commonly used primary generator is `G4ParticleGun`, and it’s the one used in this work as well.

G4ParticleGun does not present any randomisation in itself, but C++ methods can be employed to create any desired distribution.

After the primary has been generated and passed, GEANT4 follows it until its kinetic energy drops below a certain limit, or until it “disappears”, meaning it goes out of the World volume or decays into different particles. In the latter case, GEANT4 also tracks the newly created particles. All information (kinetic energy, time, volume, type of particle, etc.) about the tracks and interactions caused by an initial particle is stored within an “event” and the user can choose to write some, or all of it, in an output file. The “event” is the primary unit of simulation in GEANT4 and the whole simulation, which contains a set of events sharing the same set-up configuration, is referred to as a “Run”.

When tracking a particle, GEANT4 must take into account physical models and/or experimental data in order to accurately calculate energy losses, reaction cross sections, etc. This is achieved through the use of a physics list. There is a wide variety of physics lists and, to save on computing time, the user can choose one that contains the physical processes more relevant to their problem.

In order to better be able to inspect the simulation, GEANT4 also offers the possibility for visualisation. The user can choose the type of data they want to graphically depict (for example detector components, particle trajectories and hits, etc.) and attribute characteristics like colour. The code for the visualisation can either be given in GEANT4 via the command line or be implemented in a macro file or the executable itself. The user can also choose the type of output file and what exactly it will contain [17].

2.3 - TALYS

TALYS [18] is a computer code system very commonly used in nuclear physics. It was created and further developed for the analysis, as well as the creation, of data. In terms of analysis, TALYS is helpful since the way experiment and theory affect each other leads to a better understanding of the fundamental interactions between particles and nuclei. Experimental data can be used to tune the simulation and, in return, investigate the reliability of other experimental measurements. In cases where no experimental data are available or after the tuning of the simulation parameters, TALYS can be used for the generation of data that can then be used in nuclear technology applications, ranging from fission reactors to nuclear medicine.

The code works by simulating a projectile hitting a target nucleus and investigating all the possible reaction channels. The projectiles TALYS supports are n, p, d, t, ^3He and α particles, while for a target the user can choose any nuclide with a mass number larger than 12. Additionally, the user can also choose a target element of natural isotopic composition. Concerning the energy of the projectile, two possibilities are available: either one energy value or a number of different energies than can be defined within the input file itself by an energy range and step or in an extra file. The energy range supported is 10^{-11}MeV up to 10^3MeV .

There is a plethora of theoretical models incorporated in TALYS. These handle the calculations according to the projectile energy and the other user defined parameters. For example, the main models describing direct reactions are the optical model with different options for its potential, such as phenomenological or microscopic, and the DWBA. The code also includes several other options for handling direct reactions as well as models for the decay of a compound nucleus and preequilibrium emission. All the models along with a schematic representation of their incorporation in a TALYS calculation are summarised in Figure 2.5.

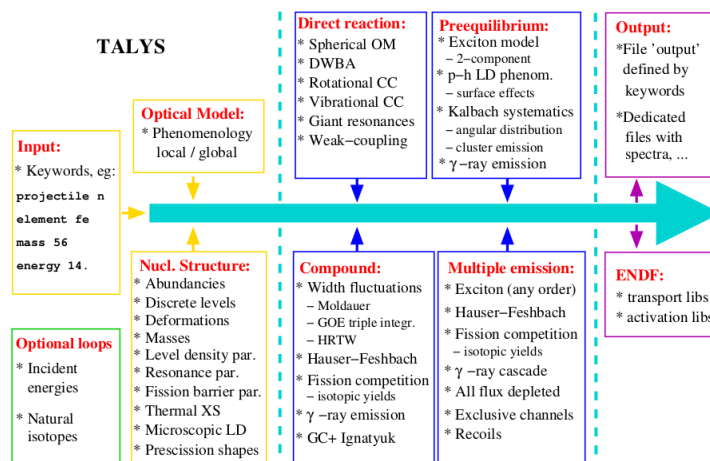


Figure 2.5: Schematic representation of the TALYS code's function along with the models used.

The variety of possible calculations and output files is very wide, from reaction cross sections, angular distributions and energy spectra to level densities to gamma ray strength functions. All these options along with their parameters can be enabled or disabled in the input file via the use of specific keywords. To save on computing time, it is advised to only enable the output files needed and choose the ejectile or residual nucleus characteristics according to the channel under study [3].

2.4 - ROOT

ROOT [19] is an object oriented framework aimed at facilitating the data analysis of High Energy Physics, but also analysis challenges of other scientific fields and even industry. It is based on the C++ programming language but is also integrated with other languages such as Python. Being object oriented reduces the code's complexity and makes modifications and extensions easier through the concepts of classes and inheritance. Furthermore, ROOT has some extra benefits coming from it being a framework, meaning that it contains existing code that the programmer can employ as-is. Thus, the programmer can use already tested and reliable code for many uses, such as fitting, histogramming, etc., while concentrating on their own problem.

ROOT provides many functionalities that a programmer needs in order to deal with the challenges of their work. It provides, for example, tools for data processing and analysis (graphs, histograms, functions, etc.) as well as for statistical analysis and visualisation (advanced graphics that can be saved in various forms, 2D and 3D plots, etc.). It also offers the possibility of data input/output and storage in forms that are easy to access and inspect but don't take up much space, such as ROOT "trees" [20].

In this work, ROOT was employed to perform many different tasks, such as plotting graphs, fitting, performing calculations etc., but the main functionality used is histogramming and, in particular, the option of creating histograms with variable bin width. The histograms that needed to be created for this study all have to do with the incident neutron energy, which lies in a range so wide that only a logarithmic axis can be used. It is thus more convenient to use bins that have a constant width not on the linear axis but on the logarithmic axis itself, so that all the range can be studied in better detail. This is sometimes referred to as "isolethargic binning" and can be expressed in a number of bins per decade (bpd), for example a histogram with 100bpd means that every order of magnitude is divided into 100 bins, i.e., the ranges 1-10MeV and 100-1000MeV alike are divided into 100 bins.

- DATA AND ANALYSIS -

- ✕ *HPGe efficiency characterisation*
- ✕ *TALYS gamma-production cross section*
- ✕ *Yield Calculation Formula*
- ✕ *GEANT4 simulation*

3.1 - HPGe efficiency characterisation

The accurate modelling of a detector by means of the GEANT4 simulation toolkit requires a series of actions from the physicist. Firstly, they have to make sure that all the parameters are optimised. This is achieved through the characterisation of the detector. During this process, the energy calibration of the detector is performed, the detection efficiency is measured with the help of a calibration source and efficiency curves are constructed. The user then tries to accurately reproduce these experimental results with the GEANT4 simulation, by tuning its parameters and comparing its results with the experimental ones.

In this work, CANBERRA's EGPC 25S/N 54035 p-type coaxial HPGe detector had to be characterised in order for the GEANT4 simulation to be employed in the calculation of the experimental counting rate of future physics experiments. The detector is shown in Picture 3.1.



Picture 3.1: The CANBERRA EGPC 25S/N 54035 p-type coaxial HPGe detector mounted on its holder.

The experimental detection efficiency data used for the characterisation were obtained in the n_TOF old Control Room at CERN, using an ^{152}Eu radioactive source. ^{152}Eu is a widely used calibration source, as it provides many γ -rays in a broad energy range. The source used in the measurements is pictured below in Picture 3.2 and its specifications are given in Table 3.1:



Picture 3.2: The ^{152}Eu radioactive source used for the detector characterisation.

Isotope	Reference Activity (kBq)	Uncertainty (%)	Active diameter (mm)
^{152}Eu	37.98	1.7	3

Table 3.1: The specifications of the calibration source.

In order to obtain spectra for different source-detector distances, several spacers were used. Their details are summarised in Table 3.2.

Label	1	2	A	B	C	D	E	F	END
Use	Source holder	Source holder	Spacer	Spacer	Spacer	Spacer	Spacer	Spacer	Spacer
S-D distance added (cm)	1	0.2	3	3	3	3	2	11	2

Table 3.2: The details of the spacers used. The label was added so that they could be distinguished during an experiment.

The measurements were performed by means of combinations of the “A”, “B”, “C”, “D”, “F” and “END” spacers with the “1” source holder. The spacers are shown in Picture 3.3. Two spectra were acquired for each distance except for the cases of 12 cm, which is a very common measuring geometry and thus 3 spectra were acquired, and that of 26 cm, which is further away from the detector and doesn’t suffer from summing effects or solid angle related problems and only one spectrum was acquired. In addition, an overnight background spectrum was acquired, in order to make sure that no background peaks coincide with the photopeaks of interest, or, if this happens, to be able to subtract them from the spectrum. All the measurements were performed at the n_TOF old control room at CERN.



Picture 3.3: The spacers used to fix the source-detector distances (left) and some of them in use (right).

The readout chain, shown in Figure 3.1, consisted of the detector’s preamplifier (PSC 736), a spectroscopy amplifier (CANBERRA 2021) and a multichannel analyser (AMETEK Pocket MCA 8000), as shown in the picture below. The voltage applied was +3000V.

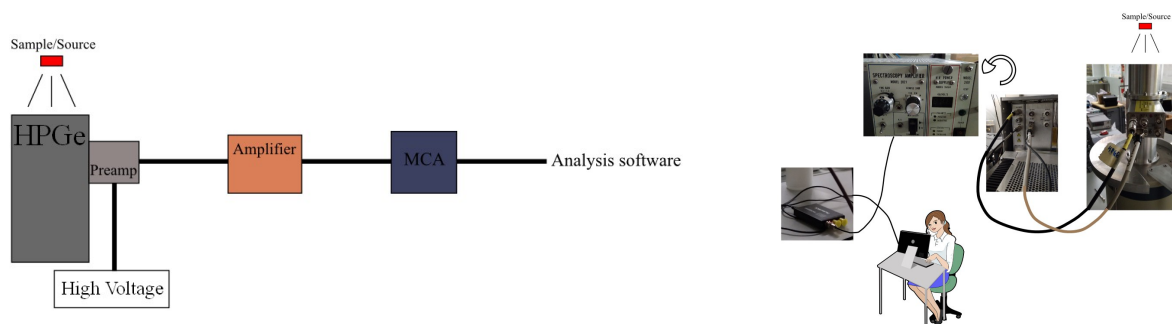


Figure 3.1: The readout chain in graphical form (left) and with the actual modules (right)

To extract the detection efficiency from the energy spectrum, one utilises the definition of a detector's efficiency, as given in paragraph 1.4, leading to

$$\text{efficiency} = \frac{\text{counts}}{\text{time} * \text{activity} * \text{intensity}}$$

where the *activity* is the source activity at the time of the measurement, *time* refers to the duration (the live time) of the measurement, *intensity* refers to the intensity of the energy peak of interest and *counts* is the total number of counts, the net area, of this particular peak.

After calculating the full-energy peak efficiency for all the γ -rays of interest, the average efficiency resulting from all the different spectra was plotted against the energy for the different source-detector distances, as shown in figure 3.2.

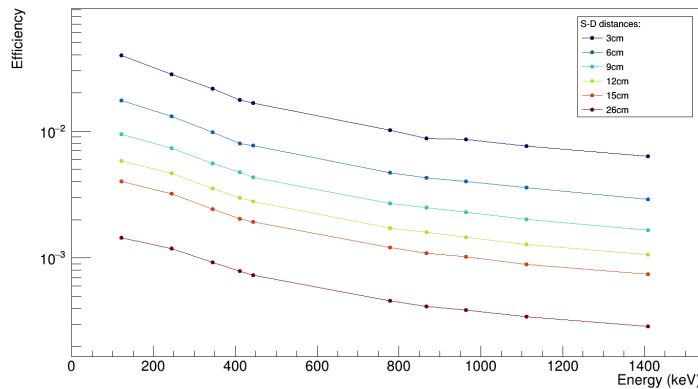


Figure 3.2: The efficiency curves for different source detector distances.

The experimental data were fitted using three different fitting functions: Linear, quadratic and polynomial [10]. An example is shown in figure 3.2. The first peak of the ^{152}Eu source (121.78 keV) is not included in the fitting process, as it lies below the point at which the efficiency curve changes behaviour (“knee” at [10], as seen in Figure 3.3). The 1085keV peak is also not used, since it cannot be clearly distinguished from its neighbouring 1089keV peak.

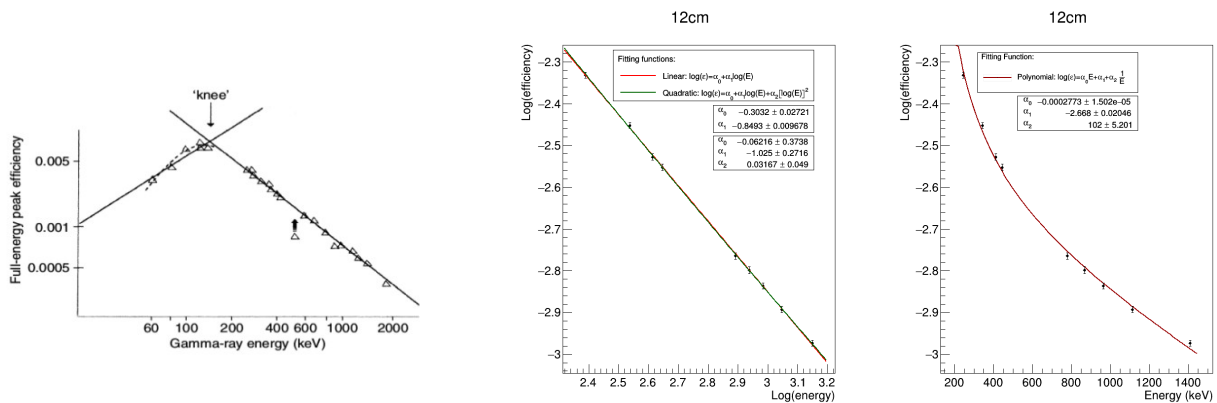


Figure 3.3: The point, referred to as “knee”, at which the efficiency changes its behaviour (left) as found in reference [10] and an example of the efficiency points fitted to the most commonly used fitting functions (right).

The final step to a full detector characterisation is its “reproduction” in a GEANT4 simulation so that this can then be used to calculate values which cannot be measured, such as the detector efficiency at different configurations and energies, or various correction factors such as target self-attenuation.

In order to achieve this, the simulation is created using the detector specifications sheet and its results are compared to the experimental ones. Apart from expected statistical discrepancies of the actual values from the specifications sheet, the detector has previously been used so it slowly starts to deteriorate and the results differ. The values of the detector characteristics must then be tuned in order to achieve maximal agreement between the experimental points and the simulation, as shown in Figure 3.4.

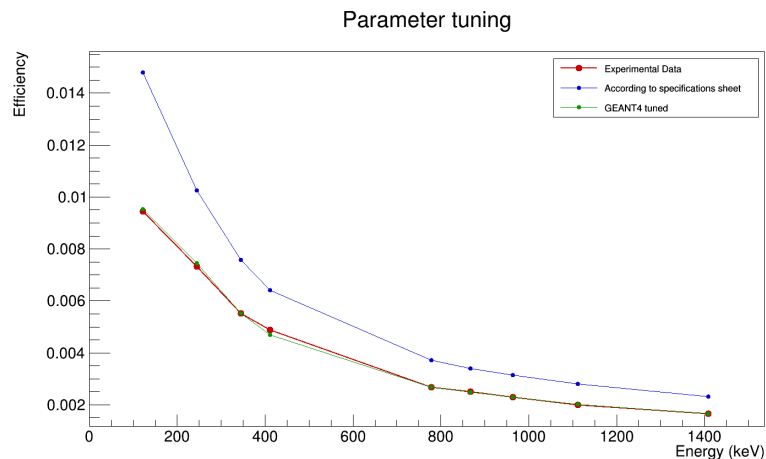


Figure 3.4: Comparison between experimental data (red) and two GEANT4 simulations: one according to the manufacturer’s specifications sheet (blue) and one after tuning the simulation values (green).

The values tuned are the values of the crystal characteristic dimensions, namely the crystal length and diameter, the thickness of its dead layer and the size of the gap, which is the distance between the Ge crystal and the detector Al housing, which is the distance between the crystal and the detector cap. When tuning, one keeps in mind that the dead layer mostly affects the low-energy γ -rays, while the length of the Ge crystal mostly affects the high-energy ones.

GEANT4 provides two methods for running the simulation. One is to simply shoot primary photons with energy corresponding to that of the γ -ray of interest and run one simulation for each photopeak. This is the monoenergetic method. The other one, the isotopic, takes the whole decay scheme of the isotope of interest into account, in this case ^{152}Eu , and runs one simulation which gives the whole spectrum as output. Both methods give the same efficiency results in relatively larger source-detector distances but, when moving the source closer to the detector, summing effects start to dominate and the monoenergetic method ceases to give accurate results. GEANT4 takes summing effects into consideration, making the isotopic method very accurate.

3.2 - TALYS gamma-production cross section

In this work, TALYS was employed in order to extract the γ -ray production cross section for the nuclear reaction in study. Calculations were performed both with the default parameters and with various different options for the theoretical models included in the package. All the results were compared to γ -production cross section experimental data, as well as total inelastic cross section experimental data as a cross-check of their validity. All the experimental data were taken from the EXFOR database [21]. The optimal agreement between calculations and experimental data was achieved by the default parameters results in the energy range of up to ~ 5 MeV. For higher incident energies, TALYS tends to underestimate the cross section value. However, since the energy region of interest for such nuclear reactions at this particular facility reaches up to ~ 10 MeV at most, this upper limit of agreement poses no problem for this feasibility study.

The exact TALYS input used is listed in Appendix A. Some of the comparative graphs are given in Figure 3.5. Furthermore, some results with different TALYS parameters can be found in Appendix B.

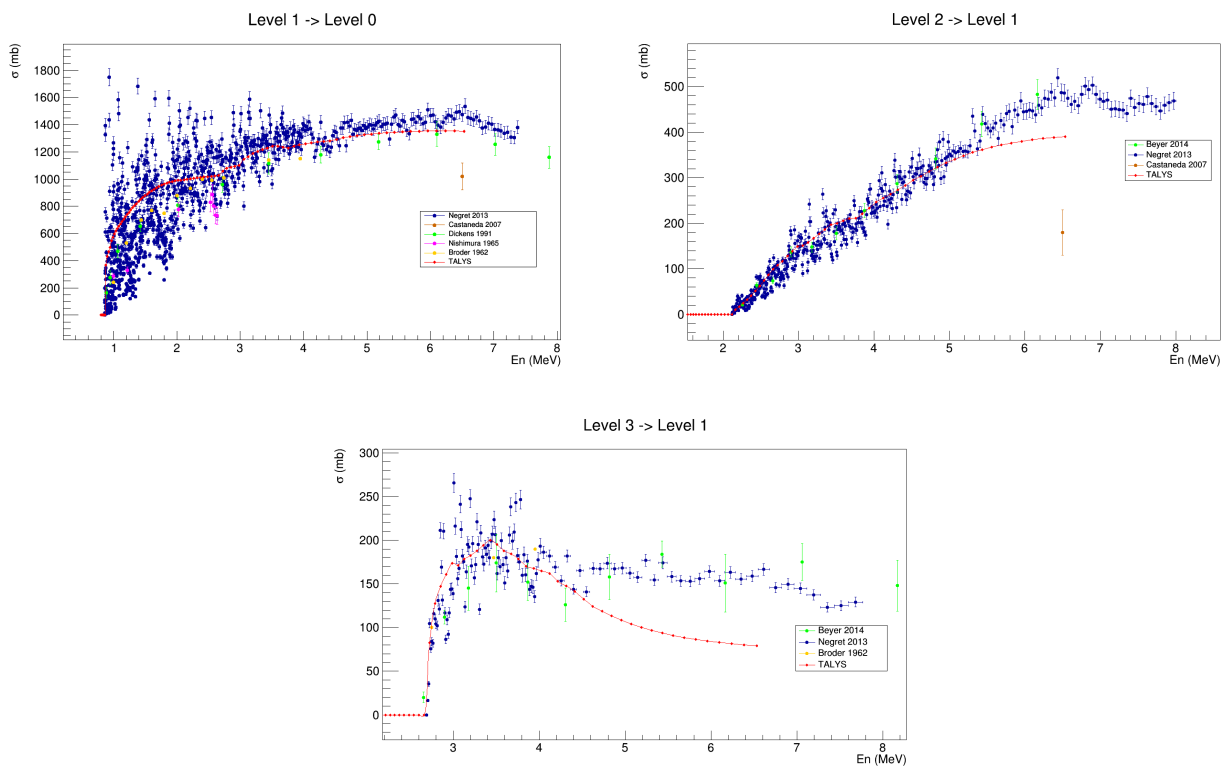


Figure 3.5: Comparison between γ -production experimental data and TALYS (in red) calculated cross section for the strongest ^{56}Fe γ -rays.

3.3 - Yield Calculation Formula

The number of photons produced by the reaction is proportional to the number of incident neutrons, to the reaction cross section, which is essentially the probability of the reaction taking place, and to the areal density of the target, which, put simply, represents how many nuclei the beam sees when hitting the target. However, of those photons produced, only a small portion will actually be recorded in the photopeak, as the detector covers a finite solid angle. Furthermore, not all photons incident on the detector fully stop within the crystal and are thus recorded in the photopeak. Taking all the above into account, the formula to calculate the recorded counts is formed as:

$$Counts = n * \frac{N_t}{target\ surface} * \epsilon_{intr} * \Delta\Omega * \frac{d\sigma}{d\omega}$$

where n is the number of incident neutrons, N_t is the number of target nuclei, ϵ_{intr} is the intrinsic efficiency of the detector, $\Delta\Omega$ the solid angle it covers and the proportionality factor $d\sigma/d\Omega$ is the differential cross section.

Using the Gaussian quadrature method (Paragraph 2.1) to relate the differential with the angle integrated cross section for one detector placed at an angle of 125° with respect to the neutron beam, we get that

$$\sigma_{tot} = 2\pi * 2 * \frac{d\sigma}{d\omega}$$

Combining this with the formula connecting the intrinsic and absolute efficiency of a detector given in paragraph 1.4, we get that the counts expected to be recorded can be calculated using:

$$Counts = n * \frac{N_A * mass_{target} * abundance}{A * target\ surface} * \epsilon_{abs} * \sigma_{tot}$$

Having the number of incident particles from the n_TOF EAR1 flux, the detector efficiency from the simulations performed with GEANT4 after having fully characterised the detector, and the angle integrated γ -production cross section from TALYS, we can calculate the expected counts for an experiment of average duration.

3.4 - GEANT4 simulation

The physical problem we want to recreate in GEANT4 is the measurement of the photons produced by the inelastic scattering of neutrons on a natural iron target at the n_TOF facility at CERN. The first thing to consider when creating the simulation is the geometry and general configuration. As discussed in paragraph 2.1, the one detector needs to be placed at an angle of 125° relative to the beam while, to match the expected counts calculations of paragraph 3.3, it should be placed at a distance of 15cm from the iron target. However, this distance is too large to provide adequate statistics in a simulation with reasonable CPU time, so it was decreased to 10cm. The visualisation of the configuration described above is pictured in Figure 3.6.

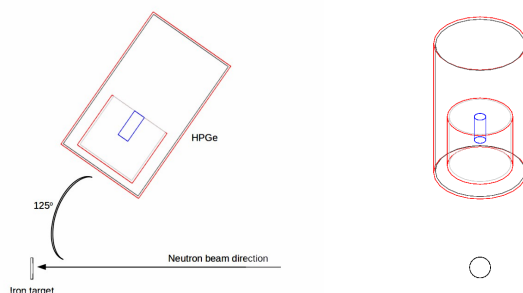


Figure 3.6: Left: Visualisation of the configuration at 90° . The HPGe is placed at a distance of 10cm from the iron target and at an angle of 125° relative to the beam. Right: From a different angle.

After having set the geometric configuration, but before we move on to creating the primaries according to the n_TOF neutron beam, it is useful to run a few tests with a monoenergetic beam of neutrons, in order to make sure that the inelastic scattering is well taken into account in the physics list that we have chosen to use (the “shielding” physics list) but also to double check the results of TALYS. A test run of 1MeV neutrons gives the spectrum depicted in figure 3.7. If we analyse this spectrum we end up with a γ -production cross section almost two times smaller than the cross section TALYS calculates. However, bearing in mind the facts that a) TALYS doesn’t exactly reproduce the experimental data and b) the experimental data available cover a big range due to the existence of resonances, especially for the first excited state decay, this result is not considered unsatisfactory.

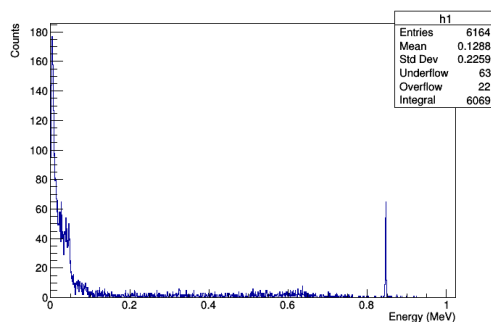


Figure 3.7: The test spectrum with a monoenergetic neutron beam of 1MeV. The ^{56}Fe first excited state decay photopeak can be clearly seen.

Following the success of the test runs comes the recreation of the n_TOF neutron beam. To do this, we need to make use of the information about the beam flux, which has been thoroughly measured, simulated [22] and written in a ROOT file as a histogram of flux vs neutron energy. This can then be easily converted into a histogram of the number of neutrons per neutron energy, which we deploy to create the simulation primaries. The histogram is given in Figure 3.8.

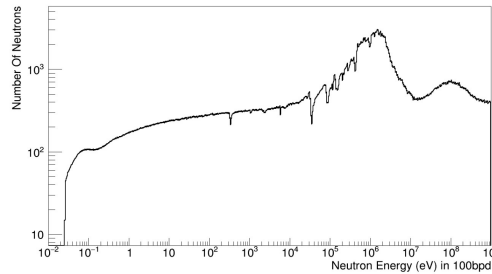


Figure 3.8: n_TOF flux per proton pulse in number of neutrons per neutron energy. Binning is 100 bins per decade.

The aim is that the run will consist of as many events as the number of neutrons produced by the proton pulses we would have in an actual experiment, with the primaries energy and number defined by the above histogram. To achieve this, we can create an external file containing the lower and the upper edge of the energy bins of the flux histogram as many times as the number of neutrons this bin corresponds to. We can then read this file in the beginning of the simulation and store these values in two global variables that can be reached by any part of the program. When the time comes for the primary generator to shoot the primaries, their energy will be taken directly from those global variables, as a random number between the bin edges. In this way the energy is chosen to be the actual energy of the n_TOF beam neutrons, while the information about their distribution is also taken into account since it is integrated in the number of lines of the input file.

The above method alone would give us the correct number of neutrons with the correct energy but all being shot at the same time. In order to accurately reproduce the experimental conditions, we would have to shoot those primaries 185m away from the target, since this is the length of the evacuated flight path. However, this would cause a considerable increase in the simulation time, so it was instead decided to calculate the time needed for the primaries to cruise the flight path and set this as their initial shooting time, but with the initial shooting point closer to the target. The calculation used is non-relativistic but this is a fairly accurate approximation, especially for the lower to medium energy range. A graph comparing the energy deposition on the detector of particles having travelled the 185m of flight path and particles that have been shot 20cm from the target but with a non-relativistically calculated initial time is depicted below, in Figure 3.9.

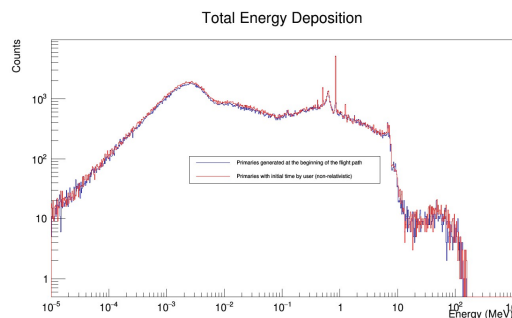


Figure 3.9: Comparison between a simulation with initial non-relativistically calculated time (red) and a simulation with an 185m evacuated flight path (blue).

Having worked on the configuration and the generation of the primaries, the simulation can be finalised and employed. The visualisation of it is given in Figure 3.10.

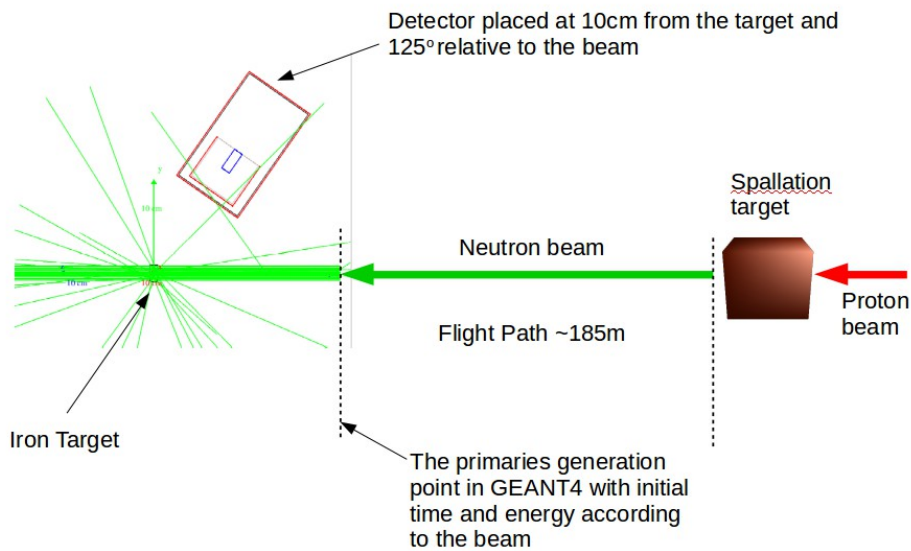


Figure 3.10: Visualisation of the GEANT4 whole simulation. Primaries are created at the initial point with an initial time given, one corresponding to the cruise of the 185m flight path after their generation by spallation at the Lead Target.

The last step to a fully operational simulation is the definition of the output we want it to provide us with. Since we are interested in the energy deposition in the detector, we must base the creation of the output file on an “if” statement that will only keep events that include a particle reaching the Ge crystal. For this work, some extra information was chosen to be written in the output file: whether the particle that enters the Ge is a photon or a neutron, distinguished by a number attributed to each particle type, the energy deposition in the crystal, the time at which the energy deposition took place, as well as the initial time and energy given to the primary that caused this event. All these were needed and incorporated so as to better be able to understand the physical processes behind the energy deposition in the detector.

The exact code fragments responsible for building the geometry, the generation of the primaries and the creation of the output file can be found in Appendix E.

- RESULTS -

☞ *Results*

The results of the detector characterisation are presented in graphical form in Figure 4.1. The red band represents the experimental uncertainty. For the two closest distances, 3cm and 6cm, the isotopic method was employed, while the results for all other distances were extracted using the monoenergetic method. For the intermediate distances, which are the most commonly adopted in experiments, the deviation between the experimentally measured and the simulated efficiency value does not exceed 2%, which equals the measurement's uncertainty.

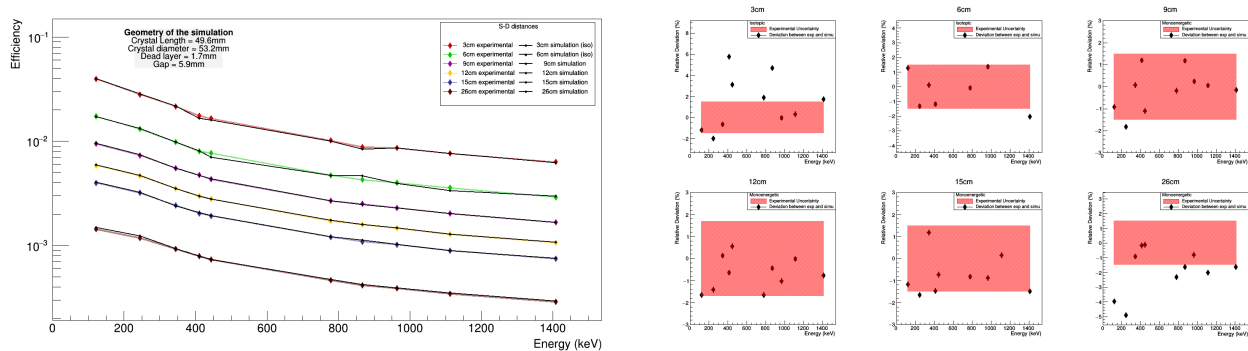


Figure 4.1: Characterisation results. Left: Efficiency curves for different source-detector distances. The black line is the simulation. Right: The deviation between experimental efficiency and simulation. Points correspond to the simulated full energy peak efficiency and the red band to the experimental uncertainty.

The optimal values for the crystal's characteristic dimensions and their deviation from the manufacturer's specifications sheet are given in Table 4.1 below:

	Specifications Sheet	GEANT4 tuned values	Deviation (%)
Crystal Length (mm)	51	49.6	2.7
Crystal Diameter (mm)	58	53.2	8.3
Dead layer thickness (mm)	0.5	1.7	240
Housing-crystal gap (mm)	4.5	5.9	31.1

Table 4.1: The final GEANT4 tuned values for the crystal's dimensions and their deviation from the values given by the manufacturer on the specifications sheet.

Using the above values for the crystal and placing the detector at an angle of 125° relative to the beam, according to the Gaussian Quadrature method, the absolute efficiency of the detector was extracted for the case of 4 γ -rays emitted after the inelastic scattering of the incident neutrons on the iron target, specifically on ⁵⁶Fe, as given in Table 4.2:

γ -ray energy (keV)	Initial Level (J^π)	Final Level (J^π)	Detection Efficiency (from the GEANT4 simulation)	Efficiency Error
846.8	2^+	0^+	0.001048	0.000007
1232.3	4^+	2^+	0.000788	0.000006
1810.8	2^+	2^+	0.000576	0.000005
2094.7	0^+	2^+	0.000518	0.000005

Table 4.2: The detection efficiency for the 4 ^{56}Fe γ -rays studied, as extracted via GEANT4 simulation

Applying the previously (paragraph 3.3) calculated formula for the expected recorded counts, we get the following graphs (Figure 4.2):

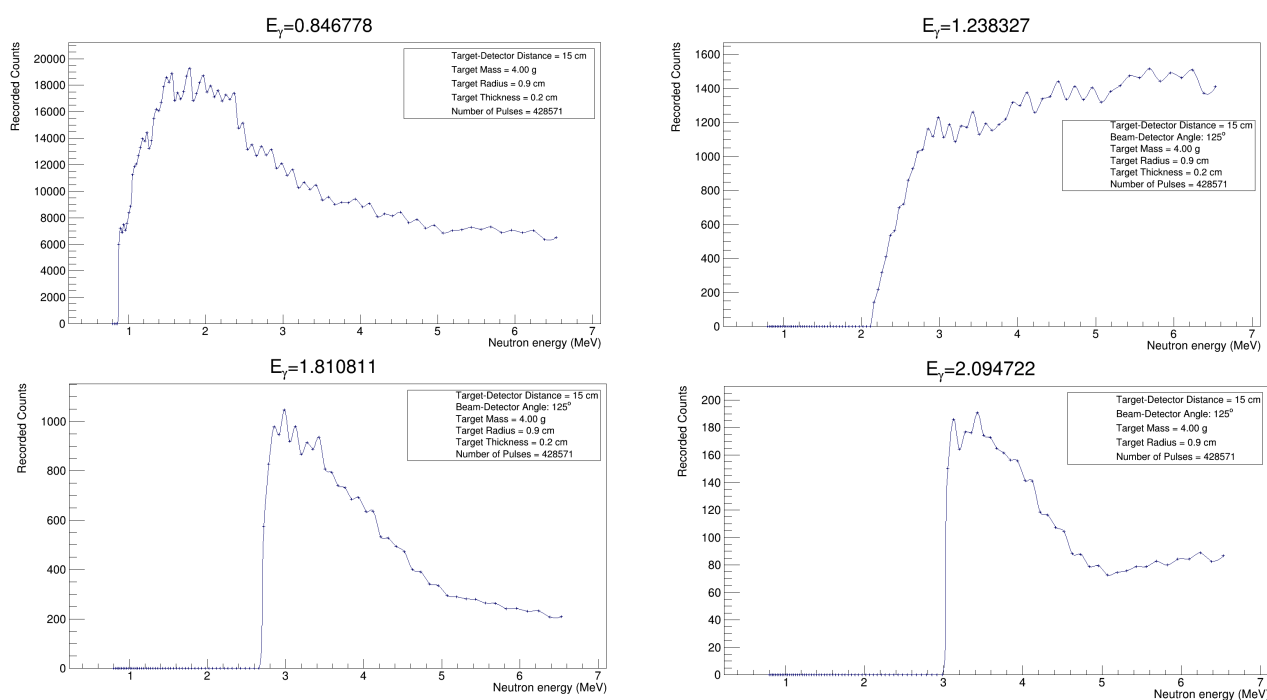


Figure 4.2: The number of counts expected to be recorded during a typical experiment of inelastic scattering of neutrons on an iron target.

Seeing how $\sim 10^3$ counts can be considered the lowest possible limit to adequate statistics, this experimental configuration can be used for the measurement of the two strongest ^{56}Fe lines at most.

After estimating the number of expected counts, we use the GEANT4 simulation to inspect the total energy deposition in the detector, taking into account all the reactions that can take place in the target, as mentioned in paragraph 1.3, as well as in the materials of the detector. For this reason, two types of histograms were created, a 1D histogram with the energy deposited in the detector on the x axis and the counts on the y, as well as a 2D histogram, with the energy of the primary particle (incident neutron) on its x axis, the energy deposition in the detector on its y axis and the counts in the z axis, represented by a colour palette. This 2D histogram is given in Figure 4.3.

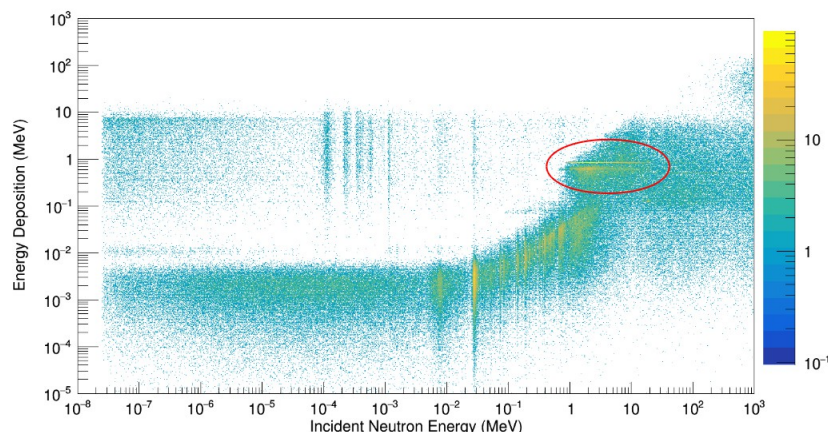


Figure 4.3: Energy deposition as a function of the incident neutron's energy represented as a 2D histogram with the incident particle's energy on the x axis and the energy deposition on the y axis. Counts are given by colour in the logarithmic z axis. The circle encloses the region of interest for the $^{56}\text{Fe}(n, n'\gamma)^{56}\text{Fe}$ reaction under study.

If we zoom in closer in the circled area we can see the lines we expected from the reaction of interest, $^{56}\text{Fe}(n, n'\gamma)^{56}\text{Fe}$.

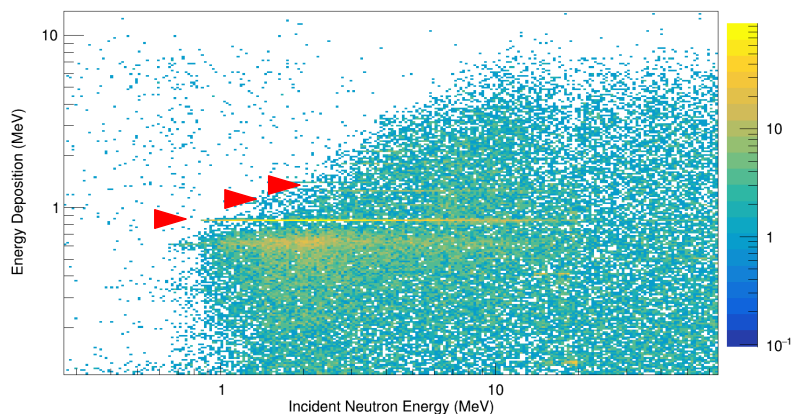


Figure 4.4: Zoom in the iron area. The red arrows point to the strongest ^{56}Fe lines

We can identify the strongest line to be the line corresponding to the decay of the 1st excited state to the ground state, seeing how it appears suddenly after a specific energy, which is the same as this decay's threshold energy, i.e. 0.847 MeV. In the same manner, we can identify the second line as the decay of the 2nd excited state to the 1st, but less clearly due to the low statistics of the simulation.

We can also see a blotch of energy deposition below the first line. This is energy deposited by photons created by neutron capture of Ge as well as the continuum we expect from the photons that reached the detector but did not deposit all of their energy within it. In order to double check the latter, we can calculate the energy value at which we expect the first iron line's Compton Edge to appear. Doing this, we get the value of 0.65MeV, which is in accordance with the appearance of this blotch of energy deposition.

In order to better be able to explain all the lines that appear in the histogram, it is useful to distinguish between energy deposition caused by a photon reaching the detector and energy deposition caused by a neutron reaching the detector. The two histograms that result from this distinction are pictured below in Figure 4.5 and the strongest lines that appear are numbered and

explained. The simulation is created with fewer statistics than the calculation of the expected recorded counts, due to computing limitations.

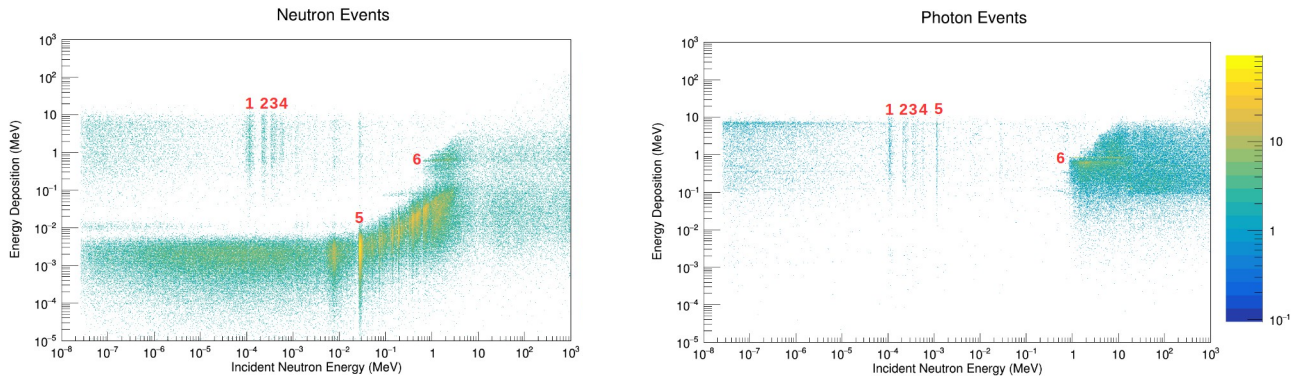


Figure 4.5: Distinction between energy deposited in events caused by neutrons hitting the detector (left) and events caused by photons hitting the detector (right). It must be noted that neutron events also contain energy deposited by photons, only photons created by neutron capture later in the event.

In the left histogram, the one containing the events caused by neutrons entering the crystal, lines number 1-4 correspond to energy deposition due to (n, γ) reactions on the Ge of the crystal. The incident particle energy at which these lines appear is the same energy where the $\text{Ge}(n, \gamma)$ cross section exhibits peaks itself. In the same way, line number 5 appears exactly at the energy where the elastic cross section on ^{56}Fe becomes significant, with the energy deposition lines at higher incident energies corresponding to elastic cross section peaks as well. These peaks of the elastic cross section are actually resonances, appearing because the energy of the incident neutrons is very low, thus the compound nucleus is the dominant reaction mechanism. When the energy of the incident neutron exactly matches the energy of a compound nucleus' excited state, the reaction cross section increases rapidly and a resonance can be seen. Line 6 and similar lines in the same area are caused by the capture of neutrons by Ge isotopes of the crystal but correspond to the energy of the photons emitted after the capture.

The cross section for the $\text{Ge}(n, \gamma)$ as well as for the elastic scattering on ^{56}Fe is pictured in Figure 4.6, as taken from the ENDF library [23].

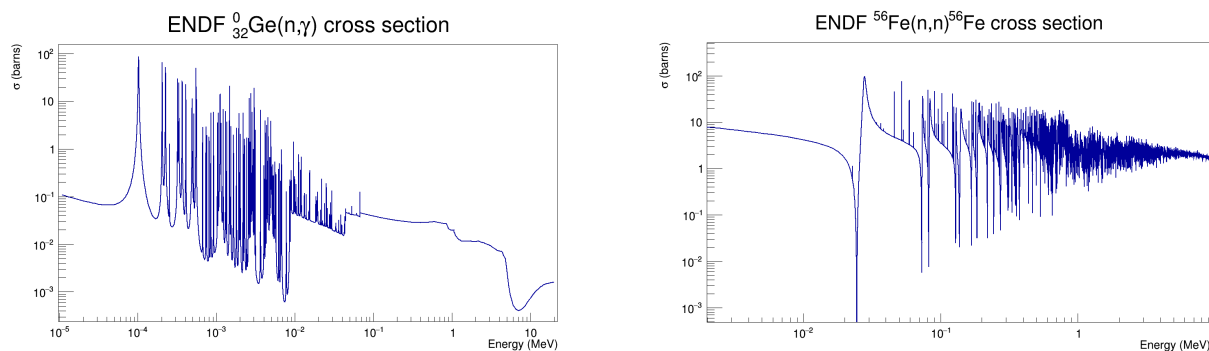


Figure 4.6: The cross section for the $\text{Ge}(n, \gamma)$ (left) and for the elastic scattering on ^{56}Fe (right), as taken from the ENDF library.

Returning to the energy deposition 2D histograms, we focus on the right graph of Figure 4.5, which gives the energy deposition by photons reaching the detector. Lines 1-4 are again due to neutron capture on the crystal. This happens because the code used to distinguish photon and neutron events asks for the type of particle when this is in the dead layer of the crystal and moves into the active volume. Thus an incident neutron can be captured within the dead layer itself and

cause a photon to be created and passed to the active volume, resulting in it being registered in the “photon events” histogram. Line 5 corresponds to a peak of the $^{56}\text{Fe}(n, \gamma)$ reaction cross section and the lines in area 6 are the lines coming from the $^{56}\text{Fe}(n, n'\gamma)^{56}\text{Fe}$ reaction, as analysed above.

The $^{56}\text{Fe}(n, \gamma)$ reaction cross section, as taken from the ENDF library, is given in Figure 4.7.

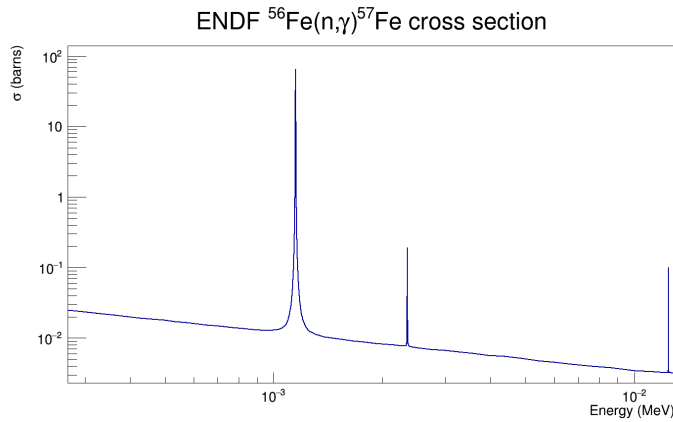


Figure 4.7: The $^{56}\text{Fe}(n, \gamma)^{57}\text{Fe}$ reaction cross section as given in the ENDF library

After using the 2D histogram to recognise and interpret the lines of higher energy deposition, we can look to the 1D histogram, given in Figure 4.8, in order to inspect them quantitatively.

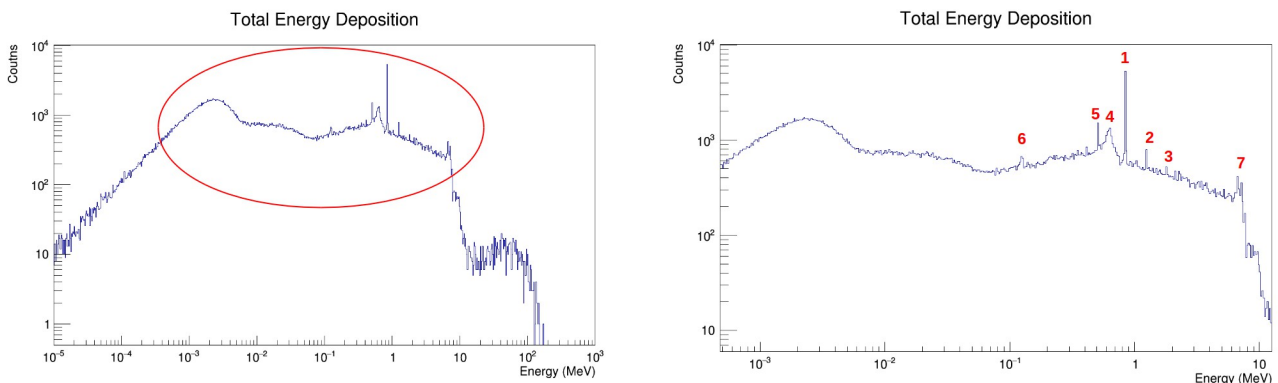


Figure 4.8: The energy deposition in the crystal (left) and the most prominent peaks (right), after zooming in the circled area of the left histogram

If we zoom in the circled region of the total energy deposition histogram, we can recognise the first three ^{56}Fe peaks (peaks number 1, 2 and 3) as well as the peaks coming from the photon energy deposition after neutron capture on Ge (peak number 4, which corresponds to the energy of the de-excitation of excited states of Ge isotopes but also peak number 7, corresponding to the Q-value of the capture reaction). We can also clearly see the annihilation peak at 0.511 MeV (peak number 5), resulting from electron and positron interaction. The last peak of the spectrum is peak number 6, that matches the characteristic Ge X-rays as well as the decay of ^{57}Fe first excited state. We can see that the strongest iron line can be very well distinguished from the background, even with the lower statistics.

- CONCLUSIONS -

☒ *Conclusions*

In this work, the installation and design of a γ spectrometry set-up in the n_TOF facility at CERN was investigated through simulations with the GEANT4 toolkit and the TALYS code. CANBERRA's EGPC 25S/N 540 p-type coaxial prototype HPGe was characterised in terms of its efficiency using a ^{152}Eu calibration source. The characterisation, accurate within 2% for the commonly used source-detector distances of 6cm, 9cm, 12cm and 15cm, was then used to calculate the efficiency of the detector for a different geometrical configuration and for the energies of the first few γ -rays resulting from the decay of ^{56}Fe to its ground state. This was needed in order to estimate the number of counts expected to be recorded in a real-life inelastic scattering experiment. The production cross section of these γ -rays was determined by statistical model calculations via the TALYS code. The estimated recorded counts reached a maximum of $\sim 10^4$ counts for the decay of ^{56}Fe first excited state and decreased for the rest of the γ -rays under study. The statistics can be improved by introducing a second detector to the set-up. Performing a GEANT4 simulation of the whole case allowed for an inspection of the expected background, which consisted mostly of energy deposition due to elastic scattering and neutron capture on both the target and the detector materials.

Some improvements on this study could be the inclusion of the angular distribution of the γ -production cross section, a more detailed simulation and better efficiency calibration of the detector.

- REFERENCES -

☞ *References*

- [1]: K. S. Krane, *Introductory Nuclear Physics*, John Wiley and Sons, 1988
- [2]: M. LeBellac, *Quantum Physics*, Cambridge University Press, 2006
- [3]: TALYS User Manual
- [4]: L.C. Mihailescu, L. Oláh, C. Borcea, A.J.M. Plompen, A new HPGe setup at GELINA for measurement of gamma-ray production cross-sections from inelastic neutrons scattering, *Nucl. Instrum. Methods Phys. Res. A*, 531 (2004) 375
- [5]: L.C. Mihailescu, C. Borcea, A. Koning, A.J.M. Plompen High resolution measurement of neutron inelastic scattering and cross-sections for ^{52}Cr , *Nucl. Phys. A*, 786 (2007), pp. 1-23
- [6]: L.C. Mihailescu, C. Borcea, et al., A measurement of (n, xn γ) cross-sections for ^{208}Pb from threshold up to 20MeV, *Nucl. Phys. A*, 811 (2008), pp. 1-27
- [7]: <https://www.nndc.bnl.gov/> [last visited on 06/02/2020]
- [8]: G. F. Knoll, *Radiation Detection And Measurement*, John Wiley and Sons, 2000
- [9]: W. R. Leo, *Techniques for Nuclear and Particle Physics Experiments – A how to approach*, Springer-Verlag, 1987
- [10]: G. R. Gilmore, *Practical Gamma-ray Spectrometry*, 2nd Edition, John Wiley & Sons, 2008
- [11]: K. Debertin and R. G. Helmer, *Gamma- and X-ray spectrometry with semiconductor detectors*, Elsevier, 1988
- [12]: <https://ntof-exp.web.cern.ch/ntof-exp/> [last visited on 21/01/2020]
- [13]: K. E. Atkinson, *An introduction to numerical analysis*, 2nd edition, John Wiley and Sons, 1989
- [14]: C. Petrone, Detector Kick-Off Meeting presentation, CERN, 10/04/2019
- [15]: <https://geant4.web.cern.ch/> [last visited on 25/01/2020]
- [16]: Agostinelli S. et al, Geant4 – a simulation toolkit, *Nucl. Instr. Meth. Phys. Res. A*, 506, 3, (2003), 250-303.
- [17]: GEANT4 User's Guide: For Application Developers
- [18]: https://tendl.web.psi.ch/tendl_2019/talys.html [last visited on 17/02/2020]
- [19]: <https://root.cern/> [last visited on 22/02/2020]
- [20]: ROOT User's Guide
- [21]: <https://www.nndc.bnl.gov/exfor/> [last visited on 06/02/2020]
- [22]: Sabaté-Gilarte, M., Barbagallo, M., Colonna, N. *et al.* High-accuracy determination of the neutron flux in the new experimental area n_TOF-EAR2 at CERN. *Eur. Phys. J. A* **53**, 210 (2017)
- [23]: <https://www.nndc.bnl.gov/exfor/endlf00.jsp> [last visited on 06/02/2020]

- APPENDICES -

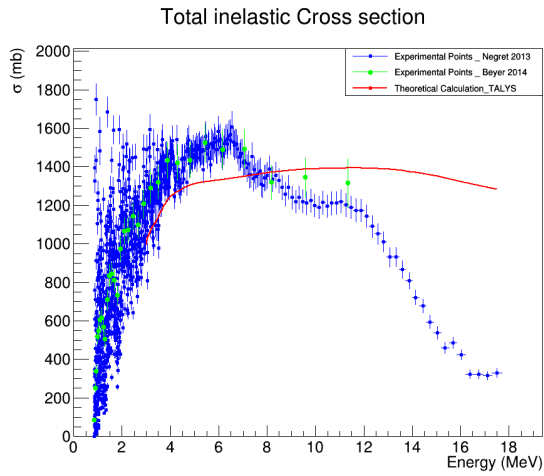
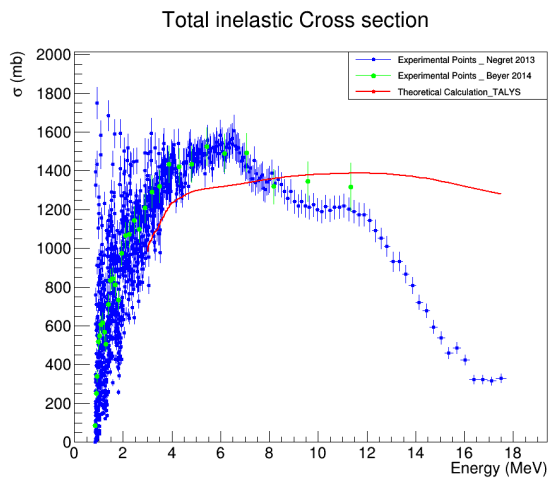
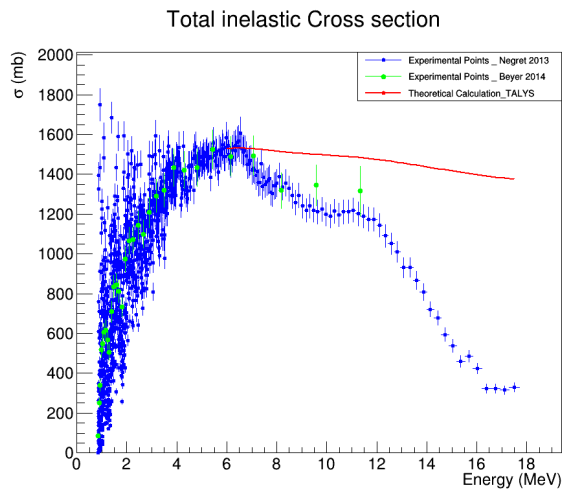
- ✎ *Appendix A*
- ✎ *Appendix B*
- ✎ *Appendix C*
- ✎ *Appendix D*
- ✎ *Appendix E*

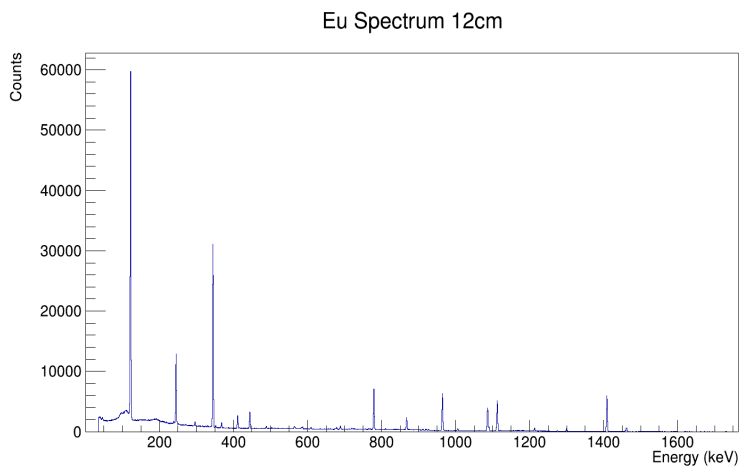
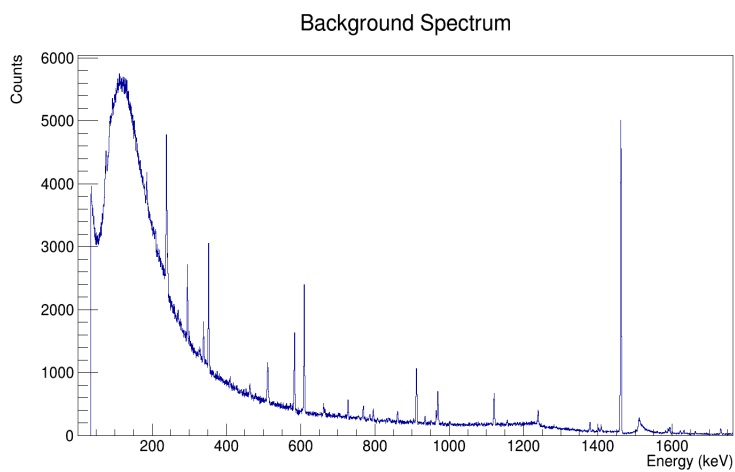
TALYS code input

```
##### BASIC INPUT #####
projectile n
element fe
mass 56
energy energies

##### OUTPUT #####
ejectiles n,g
maxZ 0
channels y
outgamdis y
```

Projectile:	Defines the incident particle type
element:	Defines the target element
mass:	Defines the target element's mass number
energy:	Provides the incident particle's energy (in this case through an external file)
ejectiles:	Defines the type of outgoing particles (used to save on computing time)
maxZ:	Defines the atomic number of the residual nuclide that is the furthest away from the initial compound nucleus and that will be the last residual to be studied in this chain (in this case maxZ = 0, so only iron isotopes are studied)
channels:	Flag that indicates the output of all reaction channels
outgamdis:	Flag that indicates the output of discrete γ -ray intensities

Microscopic Optical Model Potential (mode 1)Microscopic Optical Model Potential (mode 2)Without taking pre-equilibrium emission into account

Example ^{152}Eu Spectrum for efficiency calculationnTOF old control room overnight Background Spectrum

Calculation of Expected Recorded Counts

```
double emissions[92];  
for (int i=0; i<92; i++) {  
    emissions[i]=(number_of_neutrons[i]/target_surface)*number_of_target_nuclei*cross_section_cn2[i]*number_of_pulses;  
}  
|  
double efficiency=0.00104795;  
//The actual yield:  
double yield[92];  
for (int i=0; i<92; i++) {  
    yield[i]=emissions[i]*efficiency;  
}
```

GEANT4 code fragments regarding the:**1) reading of the flux file and storing its information**

```

//Global variables:
G4double Depos; // The energy deposition in my detector
G4double Energy[569641]; // The energy I want to give to my primaries
G4double time_ns; // The time I want to give to my primaries (in ns)
G4int particle_type; // What type of particle I have.
                    // photon = 1
                    // neutron = 2
                    // otherwise = 0
G4double Edge1[569641], Edge2[569641];
G4double global_time; // Time since the event was created (ns by default)
G4int evtNo;

int main(int argc, char** argv) {

    // reading the input file to keep the globals in memory
    std::ifstream infile;
    infile.open("data_one_pulse_edges.txt", std::ios::in);

    for (G4int i=0; i<569641; i++) {
        infile >> Energy[i] >> Edge1[i] >> Edge2[i];
    }

    infile.close();
}

```

2) placing and rotating of the detector

```

G4RotationMatrix* xRot = new G4RotationMatrix;
xRot->rotateX(-M_PI/3.27*rad);

G4ThreeVector zTrans(0, 13.7676*cm, -9.6277*cm);

G4VPhysicalVolume *ALTube_phys
= new G4PVPlacement(xRot, zTrans,
                    AL_log, "ALTube", World_log, false, 0);

```

3) generation of the Primaries

```

void XriPrimaryGeneratorAction::GeneratePrimaries(G4Event* anEvent) //
{
    G4double px0=0., py0=0., pz0=+1.;
    fParticleGun->SetParticleMomentumDirection(G4ThreeVector(px0, py0, pz0));

    G4double x0=0.*cm, y0=0.*cm, z0=-20.0*cm;
    // G4double thickness=0.122*cm; // source thickness
    G4double rho=0.9*cm;
    //G4double dz0=0.2*cm;
back:
    x0 = rho*(1.-2.*G4UniformRand());
    y0 = rho*(1.-2.*G4UniformRand());
    if ((x0*x0+y0*y0)>(rho*rho)) goto back;

    fParticleGun->SetParticlePosition(G4ThreeVector(x0, y0, z0));

    G4int matrix_element_no = fmod(evtNo, 569641);
    G4double central_energy = Energy[matrix_element_no];
    G4double low_edge = Edge1[matrix_element_no];
    G4double upper_edge = Edge2[matrix_element_no];

    G4double energy = G4RandFlat::shoot(low_edge, upper_edge);

    fParticleGun->SetParticleEnergy(energy);

    // To Give Time:
    // 185m flight path:
    G4double c=299792458.0; // m/s
    G4double neutron_mass=939.56378; //MeV/c2

    G4double time_s;
    time_s = sqrt(neutron_mass*185.*185./(2.*energy*c*c));
    time_ns = time_s*1e9;

    fParticleGun->SetParticleTime(time_ns);
}

```

4) creation of the output file

```

if (currentVolume1!=NULL) {
  if (currentVolume1->GetName() == "GeTube")
  {
    if(aStep->GetTotalEnergyDeposit(>0) {
      fprintf(opfp, "%9d %10.6e %20.10e\n", evtNo+1, aStep->GetTotalEnergyDeposit(), aStep->GetTrack()->GetGlobalTime()/s);
    }
    Depos += aStep->GetTotalEnergyDeposit();
  }
}

//=====
std::ofstream gammas;
std::ofstream neutrons;

gammas.open("gammas.dat", std::ios::app);
neutrons.open("neutrons.dat", std::ios::app);

if(particle==G4Gamma::Definition() && currentVolume1->GetName()=="outDeadTube" && aTrack->GetNextVolume()->GetName()=="GeTube") {
  gammas << evtNo+1 << G4endl;
  particle_type=1;
}

if(particle==G4Neutron::Definition() && currentVolume1->GetName()=="outDeadTube" && aTrack->GetNextVolume()->GetName()=="GeTube") {
  neutrons << evtNo+1 << G4endl;
  particle_type=2;
}

} // First if: Current volume != NULL

```


Maria-Elisso Stamati

Postgraduate Student

Department of Physics, University of Ioannina
